



Calhoun: The NPS Institutional Archive
DSpace Repository

Theses and Dissertations

1. Thesis and Dissertation Collection, all items

1975

Characterizing and controlling the
metallurgical properties of a Cu-Mn alloy for
ship silencing applications.

Youngblood, Frederick Lee

Monterey, California. Naval Postgraduate School

<http://hdl.handle.net/10945/20774>

Downloaded from NPS Archive: Calhoun



Calhoun is the Naval Postgraduate School's public access digital repository for research materials and institutional publications created by the NPS community. Calhoun is named for Professor of Mathematics Guy K. Calhoun, NPS's first appointed -- and published -- scholarly author.

Dudley Knox Library / Naval Postgraduate School
411 Dyer Road / 1 University Circle
Monterey, California USA 93943

<http://www.nps.edu/library>

CHARACTERIZING AND CONTROLLING
THE METALLURGICAL PROPERTIES OF
A Cu-Mn ALLOY FOR SHIP SILENCING
APPLICATIONS

Frederick Lee Youngblood

Library
Naval Postgraduate School
Monterey, California 93940

NAVAL POSTGRADUATE SCHOOL

Monterey, California



THESIS

CHARACTERIZING AND CONTROLLING THE
METALLURGICAL PROPERTIES OF A
Cu-Mn ALLOY FOR SHIP SILENCING
APPLICATIONS

by

Frederick Lee Youngblood

June 1975

Thesis Advisor:

G. Edwards

Approved for public release; distribution unlimited.

T168216

| REPORT DOCUMENTATION PAGE | | READ INSTRUCTIONS BEFORE COMPLETING FORM |
|---|-----------------------|---|
| 1. REPORT NUMBER | 2. GOVT ACCESSION NO. | 3. RECIPIENT'S CATALOG NUMBER |
| 4. TITLE (and Subtitle) CHARACTERIZING AND CONTROLLING THE METALLURGICAL PROPERTIES OF A Cu-Mn ALLOY FOR SHIP SILENCING APPLICATIONS | | 5. TYPE OF REPORT & PERIOD COVERED Master's Thesis; June 1975 |
| 7. AUTHOR(s) Frederick Lee Youngblood | | 6. PERFORMING ORG. REPORT NUMBER |
| 9. PERFORMING ORGANIZATION NAME AND ADDRESS Naval Postgraduate School Monterey, California 93940 | | 8. CONTRACT OR GRANT NUMBER(s) |
| 11. CONTROLLING OFFICE NAME AND ADDRESS Naval Postgraduate School Monterey, California 93940 | | 10. PROGRAM ELEMENT, PROJECT, TASK AREA & WORK UNIT NUMBERS |
| 14. MONITORING AGENCY NAME & ADDRESS (if different from Controlling Office) Naval Postgraduate School Monterey, California 93940 | | 12. REPORT DATE June 1975 |
| | | 13. NUMBER OF PAGES 84 |
| | | 15. SECURITY CLASS. (of this report) unclassified |
| | | 15a. DECLASSIFICATION/DOWNGRADING SCHEDULE |
| 16. DISTRIBUTION STATEMENT (of this Report) Approved for public release; distribution unlimited. | | |
| 17. DISTRIBUTION STATEMENT (of the abstract entered in Block 20, if different from Report) | | |
| 18. SUPPLEMENTARY NOTES | | |
| 19. KEY WORDS (Continue on reverse side if necessary and identify by block number) | | |
| 20. ABSTRACT (Continue on reverse side if necessary and identify by block number) Electrical resistivity measurements were used to investi- gate the effect of stress, applied during aging and quenching, on the specific damping capacity (SDC) of Incramute (a 40 Mn - 58 Cu - 2 Al commercial alloy). It was found that (1) stress applied during either aging, or quenching reduces the SDC of the alloy, (2) the martensitic transformation temperature is a linear function of the stress applied during quenching, and | | |

(3) stress applied during the aging treatment retards the aging kinetics. The hysteresis of the martensite transformation, and the Neel temperature were determined from resistivity-temperature data. A phenomenological model based on SDC, percent of the martensitic transformation, and applied stress was developed to describe and predict the alloy's SDC behavior under various heat treatment schemes and stress conditions.

Characterizing and Controlling the Metallurgical
Properties of a Cu-Mn Alloy for
Ship Silencing Applications

by

Frederick Lee Youngblood
Lieutenant, United States Navy
B.S.M.E., University of Idaho, 1967

Submitted in partial fulfillment of the
requirements for the degree of

MASTER OF SCIENCE IN MECHANICAL ENGINEERING

from the

NAVAL POSTGRADUATE SCHOOL
June 1975

ABSTRACT

Electrical resistivity measurements were used to investigate the effect of stress, applied during aging and quenching, on the specific damping capacity (SDC) of Incramute (a 40 Mn - 58 Cu - 2 Al commercial alloy). It was found that (1) stress applied during either aging, or quenching reduces the SDC of the alloy, (2) the martensitic transformation temperature is a linear function of the stress applied during quenching, and (3) stress applied during the aging treatment retards the aging kinetics. The hysteresis of the martensite transformation, and the Néel temperature were determined from resistivity-temperature data. A phenomenological model based on SDC, percent of the martensitic transformation, and applied stress was developed to describe and predict the alloy's SDC behavior under various heat treatment schemes and stress conditions.

TABLE OF CONTENTS

| | | |
|------|--|----|
| I. | INTRODUCTION | 11 |
| A. | APPLICATIONS | 11 |
| B. | METALLURGY OF Cu-Mn ALLOYS | 14 |
| C. | THE GENERAL EFFECT OF STRESS ON AGING AND QUENCHING TRANSFORMATIONS | 18 |
| 1. | Aging Effects | 19 |
| 2. | Cooling Effects | 22 |
| II. | OBJECTIVES | 26 |
| III. | EXPERIMENTAL METHODOLOGY | 27 |
| A. | SPECIFIC DAMPING CAPACITY MEASUREMENT | 28 |
| B. | ELECTRICAL RESISTIVITY MEASUREMENT | 30 |
| 1. | Resistivity as a Property | 30 |
| 2. | Resistivity Measurement | 36 |
| IV. | RESULTS AND DISCUSSION | 41 |
| A. | CORRELATION OF SDC AND RESISTIVITY | 41 |
| B. | AGING PROCESS | 43 |
| 1. | Temperature Effects | 43 |
| 2. | Stress Effects | 54 |
| C. | QUENCHING PROCESS | 58 |
| 1. | Temperature Effects | 58 |
| 2. | Stress Effects | 59 |
| D. | SDC TEST - SURFACE SHEAR STRESS EFFECTS | 64 |
| E. | BEHAVIORAL MODEL | 69 |
| F. | RESISTIVITY BEHAVIOR | 73 |
| V. | CONCLUSIONS | 76 |

| | |
|-------------------------------------|-----|
| VI. RECOMMENDATIONS | .78 |
| APPENDIX | 79 |
| LIST OF REFERENCES | 82 |
| INITIAL DISTRIBUTION LIST | .84 |

LIST OF FIGURES

Figure

| | | |
|----|--|----|
| 1 | SDC of Various Alloys as a Function of Yield Strength | 13 |
| 2 | Equilibrium Phase Diagram for Mn-Cu Alloys.... | 16 |
| 3 | Photographs of Test Equipment..... | 29 |
| 4 | Typical Torsion Pendulum Output..... | 31 |
| 5 | Photographs of Specimen Connections..... | 37 |
| 6 | Diagram of Resistivity Measurement Apparatus.. | 38 |
| 7 | Test Specimen..... | 39 |
| 8 | Change in Room-Temperature Resistivity versus Various Aging Conditions, and SDC..... | 42 |
| 9 | SDC and Electrical Resistivity Relationship... | 45 |
| 10 | Temperature-Resistivity Data for 350°C Age.... | 47 |
| 11 | Temperature-Resistivity Data for 400°C Age.... | 48 |
| 12 | Temperature-Resistivity Data for 425°C Age.... | 49 |
| 13 | Temperature-Resistivity Data for 450°C Age.... | 50 |
| 14 | Temperature-Resistivity Data for 500°C Age.... | 51 |
| 15 | Temperature-Resistivity Data for 550°C Age.... | 52 |
| 16 | Activation Energy-Aging Data..... | 55 |
| 17 | Resistivity Aging Curve, No-Stress Age..... | 56 |
| 18 | Resistivity Aging Curve, Stress-Age..... | 57 |
| 19 | Affects of Stress on Martensitic Transformation Temperature..... | 60 |
| 20 | Hysteresis Curve of Martensitic Transformation. | 63 |
| 21 | Aging Temperature Effects on SDC for Different Matrix Conditioning Treatments..... | 65 |

| | | |
|----|---|-----|
| 22 | Effect of Surface Shear Stress on SDC Test Results | .68 |
| 23 | Microstructural Model of Specific Damping Capacity in Incramute | 70 |
| 24 | Temperature-Resistivity Characteristics Used to Reflect Néel Temperature | .74 |

LIST OF TABLES

Table

| | | |
|----|--|----|
| I | Properties of Incramute | 15 |
| II | Summary of Heat Treatment Effects in Cu-Mn Alloys | 17 |

ACKNOWLEDGEMENTS

I am very grateful for the stimulating advice and guidance given by Professor Glen Edwards, to Professor Jeff Perkins for his valuable advice, and to Mr. Roy Edwards whose technical assistance greatly helped to correct many equipment problems. I would also like to thank my wife whose patience and dedicated support helped immensely.

I. INTRODUCTION

A. APPLICATIONS

Since unwanted vibrations contribute to both machine failures and human performance, the control of machine noise has long been an engineering objective. In the military domain, the control of noise sources plays a particularly important role in the search and detection relationship between surface ship and submarine, and mine warfare. The various combinations of auxiliary and propulsion machinery that are operated aboard naval vessels gives each type of ship its own characteristic acoustic signature. This has made it possible to devise weapon systems which utilize these acoustic signals for target detection, terminal guidance and warhead triggering. Ship silencing has therefore become a very important factor in ship design.

The interface in machine design between function and the reduction of machinery noise has nearly always involved compromises due to cost considerations. Several approaches to vibration reduction have been employed. These may be classified into two general areas; (1) isolation and (2) design. Isolation means that there is some mechanism used to interrupt the vibration signal. This has been accomplished by incapsulating the machinery, using vibration damping devices for machinery supports

or by locating noisy machinery in remote areas. Optimally, it is best to design unwanted vibration out of the machinery initially. This is accomplished by: (1) proper choice of materials, (2) locating resonant frequencies far away from the operating frequency, (3) avoiding large surface areas which might act as vibration amplifiers, (4) proper choice of component tolerances, (5) optimum use of power transmission devices, (6) avoiding vibrating air columns, and (7) avoiding unbalance in rotating components.

Perhaps the most involved factor in these decisions is that of material selection. Material choice has typically been mediated by the environment to which a device is subjected, and the stresses and temperatures involved in its application, with only a cursory look at its vibration damping qualities. Materials which possess the strength and vibration damping characteristics desirable in machine design have only recently become available. Figure 1 gives the relative ranking for a few materials in terms of their damping capability. Of particular interest are the Cu-Mn alloys, which exhibit very desirable strength and damping properties. The judicious employment of these alloys to take advantage of their intrinsic damping qualities should significantly reduce unwanted machine noise, while prolonging machinery life and reducing the need for costly items such as resilient isolation mounts.

Past efforts to use Cu-Mn alloys have focused on propeller design, but these alloys have not come into widespread

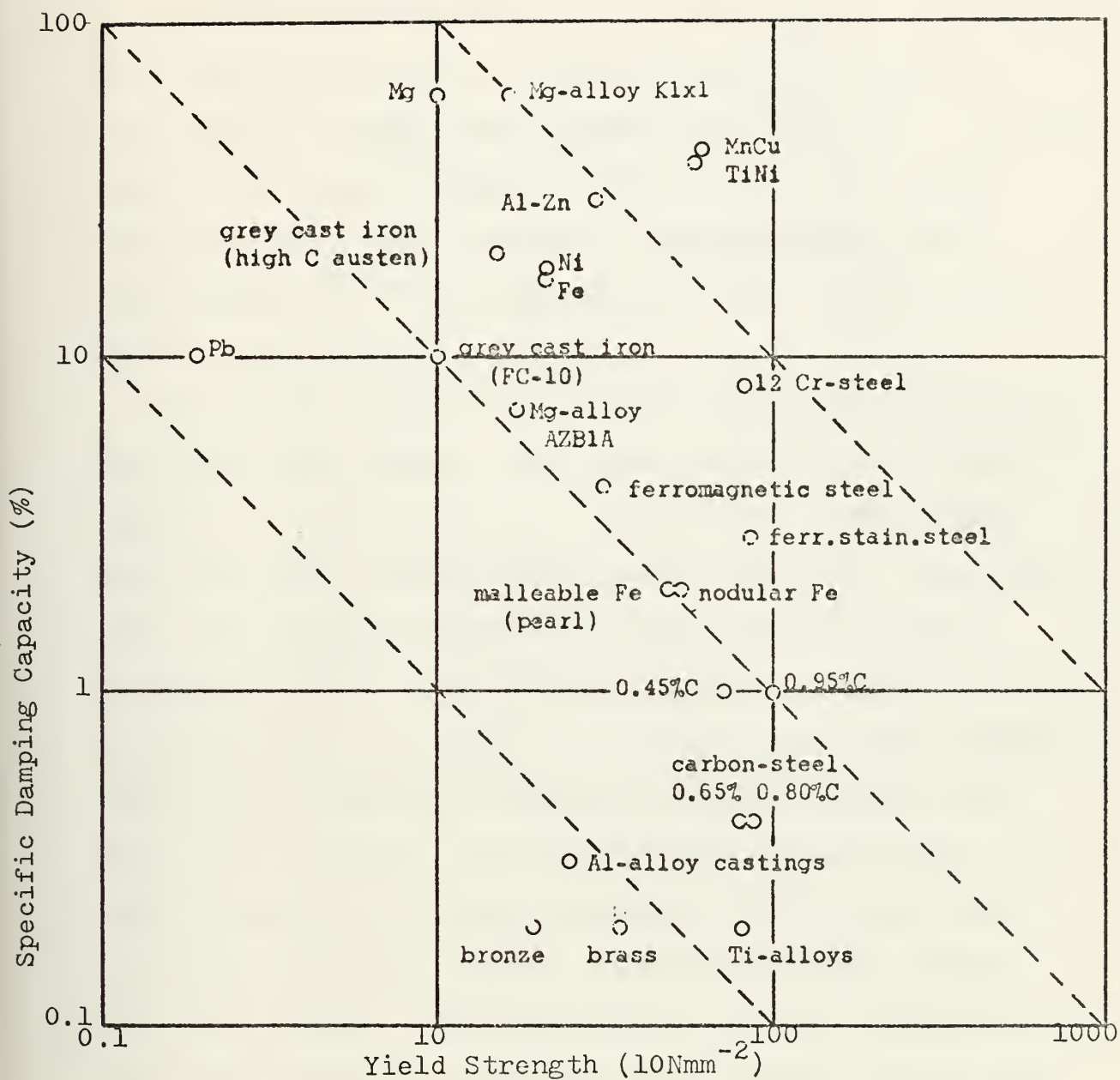


FIGURE 1. Specific damping capacity as a function of the yield stress for various materials [17] .

use due to their susceptibility to stress corrosion cracking in chloride environments [7] . Another problem associated with their use has been a marked decrease in damping capacity with increased temperature above 50°C [8] , although damping capacity is regained upon cooling. Even though new alloys with small amounts of vanadium show better performance above 50°C, this problem still remains a challenge to research [8] .

Of interest here is a relatively new alloy, "Ingramute," (Nominally 58Cu, 40Mn, 2 Al) whose properties are shown in Table I. This alloy, which is marketed by INCRA (International Copper Research Association, New York), has shown very good damping qualities with good castability and machinability [6] . Recent investigations of this alloy's characteristics have shown it to possess very good damping qualities as measured by specific damping capacity (SDC) tests [1] . However, these tests also indicated that the SDC of the alloy was highly dependent on the aging treatment given, and particularly dependent on stress during aging and cooling. This has generally been attributed to the stress-dependent, microstructural changes which occur during aging and cooling.

B. METALLURGY OF Cu-Mn ALLOYS

The Cu-Mn equilibrium diagram is given in Figure 2. Throughout this discussion and the data analysis that follows, it should be kept in mind that the heat treatments given, as shown in Table II, are not equilibrium

TABLE I. Table of physical and mechanical properties of high-damping Cu-Mn-base and Ni-Ti-base alloys, with reference properties for low-carbon steel and cartridge brass [2].

| | | "Incramute" ¹ | "55-Nitinol" | Mild Steel ² | Brass ³ |
|--------------------------------|--------------------------------|--------------------------|-------------------|-------------------------|--------------------|
| SDC | %, @ 5000 PSI | 40 | 40 | 4 | 0.2 |
| UTS | KSI | 85 | 125 ⁵ | 70 | 47 |
| YS | KSI | 45 | 25 ⁵ | 50 | 15 |
| Ductility | % elong. | 30 | 60 ⁵ | 30 | 50 |
| Modulus, E | PSI x 10 ⁶ | 12 | 12.5 ⁶ | 30 | 16 |
| Density | g/cc | 7.49 | 6.45 | | 8.53 |
| Melting point | °F(°C) | (914) | 2390 (1310) | 2775 | 1750 |
| Thermal expansion ⁴ | α μ -in/in/°C | 22.5 | 10.4 | 8.4 | 11.1 |
| Fatigue strength | KSI for 10 ⁸ cycles | 20 | 70 ⁷ | | 14 |
| Hardness | R _B (BHN) | | 90 | (140) | 65 |
| Thermal conductivity | K(BTU/ft/hr/°F) | | | 27 | 70 |
| Electrical resistivity | μ -ohm-cm | | 80 | | 6.2 |
| Electrical conductivity | % IACS@70°F | | | | 28 |
| Specific heat | BTU/lb/°F@70°F | | | .10 | .09 |
| Magnetic permeability | | | < 1 | | |

1: in optimum damping condition

2: normalized 1025 steel

3: 70-30 (cartridge) brass, annealed

4: mean coefficient, 25°C-1000°C

5: exact values dependent of test temperature relative to transition temperatures

6: of high-temperature phase

7: 10⁷ cycles

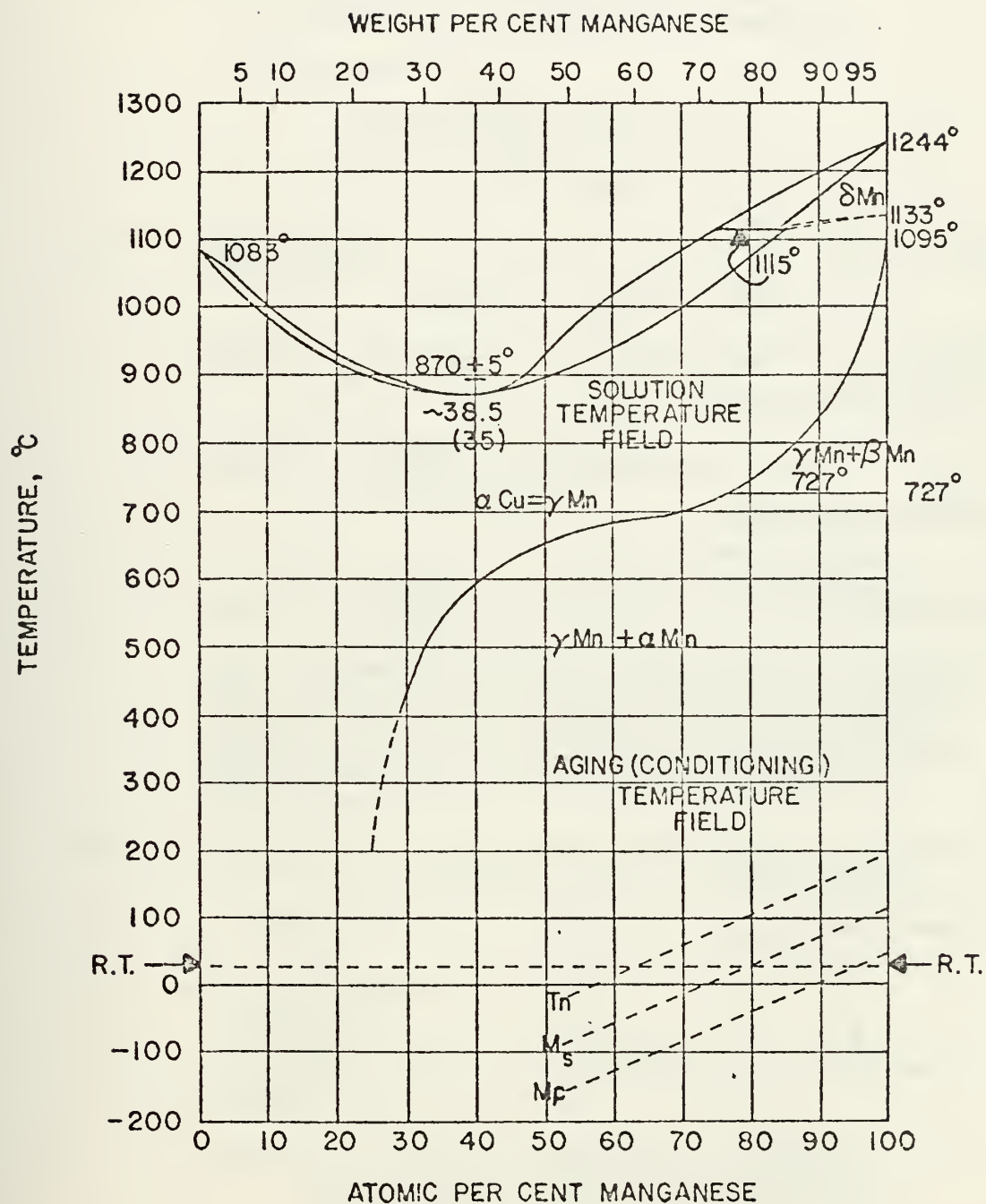
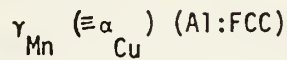


FIGURE 2. Equilibrium phase diagram for Mn-Cu alloys [2].

TABLE II. Summary of Heat Treatment Effects in Cu-Mn Alloys [2] .

Step 1: Solution treatment:

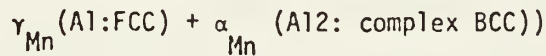


Step 2: Quench from solution treatment temperature:

If < 80 w/o Mn: γ_{Mn} retained @ room temperature

If > 80 w/o Mn: $\gamma_{\text{Mn}} \downarrow$
 antiferromagnetic ordering, @ T_N
 \downarrow
 martensitic transformation @ M_s ($T_N > M_s$)

Step 3: Aging treatment (assuming alloy < 80 w/o Mn) (in two-phase region:



Stage I: $\gamma_{\text{Mn}} \xrightarrow{\text{(initial)}} \gamma_{\text{Mn}}$ (Mn-enriched) (matrix) + " ω " (metastable Cu-rich precipitates, 100Å)

Stage II: $\xrightarrow{\text{(more time)}} \gamma_{\text{Mn}}$ (Mn-enriched (matrix) + " ω " + α_{Mn}
 (Widmanstätten precipitate)
 (small amount)

Stage III: $\xrightarrow{\text{(more time)}} \gamma_{\text{Mn}}$ (Mn-depleted) + $\xrightarrow{\text{dissolves}} \alpha_{\text{Mn}}$ (equilibrium amount)

NOTE: The condition of Stage II is typically that leading to optimum damping; Stage III is overaged, i.e. no martensitic transformation of the γ_{Mn} matrix will occur on subsequent quenching - such will occur only if the matrix is conditioned to the necessary Mn-rich state by metastable " ω " precipitation.

Step 4: Quench from the aging treatment (assuming Stage II condition from Step 3 above):

| | | | |
|--------------------------------------|--------------|---|-------------------------------------|
| γ_{Mn} (Mn-enriched) + | " ω " | + | α_{Mn} (small amount) |
| \downarrow | \downarrow | | \downarrow |
| antiferromagnetic ordering @ T_N | | | |
| \downarrow | | | |
| martensitic transformation @ M_s | retained ? | | retained |

NOTE: The martensitic transformation is triggered by the strain associated with the tetragonal distortion (FCC \rightarrow FCT) of the antiferromagnetic ordering reaction; $T_N > M_s$.

processes; but a series of highly metastable states which are very stress and temperature sensitive. The primary objective of this series of heat treatments is to obtain a conditioned microstructure with high anelastic relaxation which effectively converts vibrational energy into thermal energy.

For the solution treatment, the material (Ingramute) is heated into the "gamma" manganese ("alpha" copper) region and held for a period long enough to obtain a stabilized FCC structure; e.g., usually about 30 minutes per inch of cross-section. From this state it is water quenched to retain the δ -Mn in solution at room temperature.

The aging treatment consists of heating the material to a lower temperature (i.e., 350°C-500°C), and holding it at this temperature for a sufficient time to properly condition the matrix. This conditioning process is believed to consist of allowing Cu-rich precipitates to form, thereby leaving zones in the matrix which are Mn-rich, as indicated in Table II (Stage III).

These metastable, Mn-rich zones form the regions from which the cubic-to-tetragonal martensitic transformation occurs on cooling.

C. THE GENERAL EFFECT OF STRESS ON AGING AND QUENCHING TRANSFORMATION

Since this investigation involves both aging and cooling of Ingramute, the effect of stress on the transformations involved in the two processes will be discussed in turn.

1. Aging Effects

The aging process involves complicated diffusional processes of nucleation and growth. Since these processes occur simultaneously the relative effect of stress on each one cannot be easily quantified. However, a review of the kinetics involved will better define those parameters most likely to be affected by the application of stress.

The stress effect on the diffusion process is characterized in a general way by the relation:

$$J = - \frac{Dc}{kT} \bar{\nabla} V \quad (1)$$

where $\bar{\nabla}$ is the vector gradient of V , the potential (stress) field, D is the diffusion coefficient, c is the particular atom concentration, T is the temperature, k is the Boltzmann constant, and J is the atom flux. Factors such as the relative size of the atoms, bonding energy, atomic packing factor and lattice discontinuities determine the magnitude of the diffusivity, D , at a given temperature.

Diffusion can occur substitutionally, interstitially, along grain boundaries, or on free surfaces. Each of these processes has its own activation energy, and the process which dominates will depend on the temperature of diffusion. Generally, surface diffusion possesses the smallest activation energy; but, because the grain boundary area far exceeds the surface area in most materials, grain boundary diffusion. Lattice diffusion, or bulk diffusion, possesses the largest activation energy and generally becomes the

dominant mechanism at temperatures above $0.5 T_M$, where T_M is the melting temperature. The diffusion coefficient may be characterized by the Arrhenius relation:

$$D = D_0 e^{-Q/RT} \quad (2)$$

where D_0 is a unique diffusion constant for the particular system, Q is the activation energy, R is the universal gas constant, and T is the absolute temperature.

Since nucleation and growth processes are thermally activated, they are often experimentally characterized by utilizing the concepts of reaction rate theory. For thermally activated aging processes, a plot of the log of reciprocal aging time versus reciprocal temperature will often yield a straight line, the slope of which represents the controlling activation energy of the aging process. Processes that are competitive (parallel) will be characterized by two straight lines intersecting in a concave-upward fashion. Consecutive (series) processes are characterized by two straight lines intersecting in a concave downward fashion.

Nucleation of a new phase, like all other chemical processes, occurs when the total free energy of the system is lowered by the process. The type of phase that nucleates depends on the constituents of the solid solution, the relative size of the different atoms, and their nearest-neighbor bond strengths. For atoms of the same size, and with similar force fields, the atomic distribution of atoms

is completely random and the solution obeys Raoult's Law, i.e., the thermodynamic activity of any constituent is equal to its molefraction. This type of homogeneous solution would show no tendency to undergo a nucleation process [16] .

For solid solutions consisting of atoms of different sizes, different nearest-neighbor bond strengths or non-equilibrium solid solutions, there is a definite propensity to form unlike phases through nucleation (precipitation) reactions. The type of phases that form, and the conditions under which the transformations occur, will depend on what combinations of like or unlike atomic groupings result in the lowest free energy for the structure. This includes both the chemical free energy of the phase change, plus any accompanying strain energy and work involved in generating the new surfaces. The effect of applied stress on the reaction will enter into the energy equation as an amount of free energy.

These relationships can be characterized by the inequality:

$$F^1 - F^2 > \Delta F_c + \Delta F_s + \Delta F_{cl} + \Delta F(D,U) \quad (3)$$

where F^1 and F^2 are the chemical free energies per mole of constituents 1 and 2 respectively, and ΔF_c , ΔF_s , ΔF_{cl} , and $\Delta F(D,U)$ are the free energies per mole of constituent 2 formed corresponding to the dilational energy, interfacial energy, coherency energy of the first kind, and strain-related diffusion energy. Coherency energy of the first

kind is elastic strain energy developed by the tendency of matching phases to maintain lattice registry [15] . It should be noted that for the reaction to occur F^1 must be greater than F^2 .

In aging the Incramute alloy, the effect of stress is manifested by changes in the transformation kinetics which affect the matrix conditioning processes and subsequently, the material's ability to undergo desired transformations on cooling. In this study, the degree to which the transformation processes was affected was manifested indirectly by a resultant change in the specific damping capacity and directly by changes in the electrical resistivity of the material, two properties which are directly related to a material's structure. A very good explanation of the unstressed aging kinetics for copper-manganese alloys is given in Ref. 2.

2. Cooling Effects

Generally, the effect of the stress applied during aging is to retard or enhance the particular kinetics involved as described above. The reaction of interest during the cooling process is a martensitic type transformation; a diffusionless process which, in this case, transforms the FCC parent phase into a tetragonal structure. The transformation begins at a start temperature, M_s , and continues with decreasing temperature to completion at a temperature, M_f . The amount of the parent matrix which transforms depends on prior matrix conditioning, as

described above, and on the final temperature to which the material is cooled. Martensite forms as platelets oriented along specific shear planes in the material and are often lens shaped when viewed edge-on.

Of particular interest are the thermoelastic martensites that when heated, revert in a reversible manner to the parent phase. These martensites also have an internally twinned microstructure which is believed to be one of the chief characteristics particular to high damping materials [1] .

The formation of martensitic plates is highly directional in nature and can be influenced by stresses applied during the transformation. Again, the relationships involved can be characterized by a free energy inequality as:

$$F^D - F^m > \Delta F_e + \Delta F_s + \Delta F_{cl} + \Delta F_{c2} - U \quad (4)$$

where F^D and F^m are the chemical free energies per mole of the parent matrix and martensite respectively, ΔF_{c2} is the coherency energy of the second kind, U is the work done by applied stresses, and the other terms as previously defined. The coherency energy of the second kind is that energy which is associated with matrix shear in martensitic transformations [15] . Note that these conditions are necessary, but not sufficient, i.e., there must be regions in the parent matrix where the shear mechanism can operate before the martensitic transformation can occur.

It is also important to note that the chemical free energy imbalance required to initiate the transformation is not generally sufficient for the matrix to completely transform to martensite. Additional energy must be supplied to overcome the induced lattice strains generated by previously transformed plates of martensite, i.e., lattice accommodation strains.

The effect of applied stresses during cooling is to provide work energy to the system which acts to relieve or reinforce the lattice accommodation strains. This work function is a combination of the work done by the shear stresses and the work done by the normal stresses as they act on the martensitic plates during their formation. Thus it can be characterized by:

$$U = \tau \delta_0 + \sigma_N \epsilon_N \quad (5)$$

where τ is the applied stress resolved along the habit plane, δ_0 is the transformation shear strain, σ_N is the applied stress component normal to the habit plane, and ϵ_N is the transformation strain normal to the habit plane. The shear work is always positive due to the many potential habit planes for a material [15]. Thus, the transformation may be assisted, retarded or unaffected by applied stresses, depending on the relative signs of the terms; but in any case the shear work always assists the transformation (always positive).

The cooling processes in Cu-Mn alloys are given in step 4 of Table II. In this instance, since the

martensitic transformation is virtually time independent, air cooling was used to facilitate the measurement of the specimen's electrical resistivity. The martensitic transformation of the conditioned matrix is believed to be intimately associated with the damping characteristics of Inframute. Thus, the amount of the parent phase which transforms into martensite during cooling is directly related to the aging treatment and applied stresses during aging or cooling.

II. OBJECTIVES

The primary objective of this research was to determine the effect of stress, applied during the heat treatment processes, on the specific damping capacity of Incramute. This task was divided into two specific goals. The first goal was to identify the effect of stress on the aging process, and the second goal was to identify the effect of stress on the quenching process. Electrical resistivity was chosen to monitor the material's transformation kinetics because of the relative ease of measuring changes in this parameter with temperature. It was also desired to establish this property's relationship to the SDC of Incramute. The materials resistivity could then be used as a parameter to identify the effects of stress on the transformations involved during the aging and quenching processes.

III. EXPERIMENTAL METHODOLOGY

The technique employed to obtain data for this research consisted of maintaining a continuous record of specimen resistance versus temperature throughout various aging and quenching schemes. Each heat treatment cycle was followed immediately by a test of specimen SDC at room temperature. The total effort consisted of three specific test series aimed at elucidating the effects of stress on the aging and quenching of Incramute. All tests were made using 120-min age at temperatures greater than 350°C for the following temperatures: 350, 400, 425, 450, 500, and 550°C. Each aging treatment test was preceded by a solutionizing treatment at 700°C for 40 minutes, and followed by a forced-air quench to room temperature (22°C). Test series I consisted of no-stress tests. Test series II consisted of a tensile stress (3% of yield strength) applied during the aging process. Test series III consisted of a tensile stress (3% Y.S.) applied during the forced-air quenching process.

Two special tests were made consisting of a 425°C no-stress age for 120 minutes, an air quench under tensile stress (6% Y.S.), followed by (1) a no-stress reheat to 200°C, and (2) a reheat to 200°C under stress. These were made to obtain hysteresis data on the martensitic transformation. Also, another test consisting of heating

without stress to approximately 700°C was made in an effort to identify the Néel temperature of Incramute.

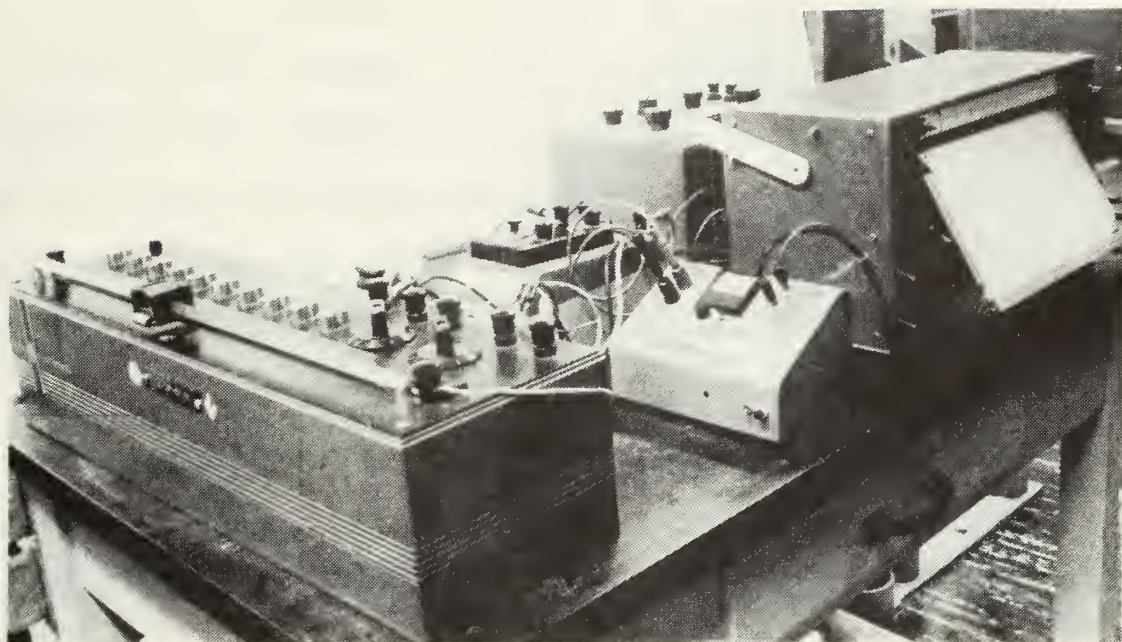
Previous testing showed good repeatability for SDC test results from different specimens indicating that properties did not vary significantly between specimens. This allowed several specimens to be used for more than one test, eliminating restarts due to damaged specimens.

A. SPECIFIC DAMPING CAPACITY MEASUREMENT

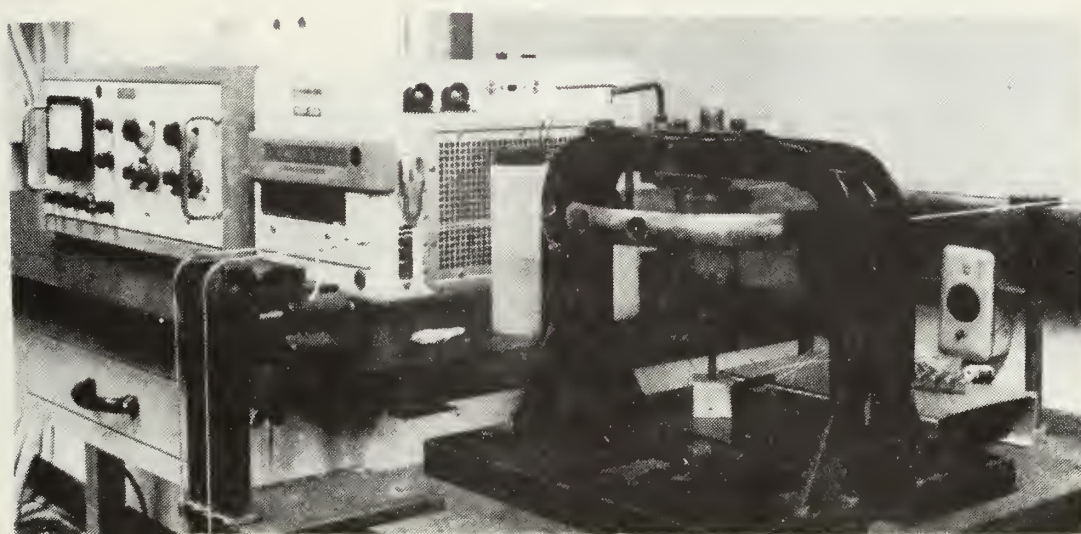
The procedure employed to measure damping capacity was based on the torsional pendulum apparatus shown in Figure 3b. This system measures damping capacity of a specimen by measuring successive amplitudes of the specimen's free vibrations following its release from an initial angular displacement. The angular displacement was varied by using various known weights with the pulley system shown. The angular displacements used corresponded to three surface shear stress levels: 1000, 5000 and 10,000 psi.

Measurement of the specimen amplitude was made by attaching a strain gage to the specimen midpoint and recording its resistance changes with a Honeywell signal amplifier and visicorder. The specific damping capacity was then taken from the visigraphs according to the formula:

$$SDC = \frac{A_1^2 - A_n^2}{NA_1^2} \times 100 \quad (6)$$



(a)



(b)

FIGURE 3. Experimental apparatus (a) resistivity measurements and (b) SDC measurements.

where A_1 and A_n are the amplitudes of the initial cycle and n th cycle, and N is the number of cycles from A_1 and A_n . This formula makes the well verified assumption that the vibrational energy is proportional to the square of the amplitude, and that the change in amplitude is proportional to the amount of energy dissipated between the cycles (see Figure 4). Engineering measurements of SDC of this type are highly stress dependent, yielding slightly different results from torsional stress than from bending stress. However, the torsional pendulum method used here yields widely accepted and rather easily correlatable results.

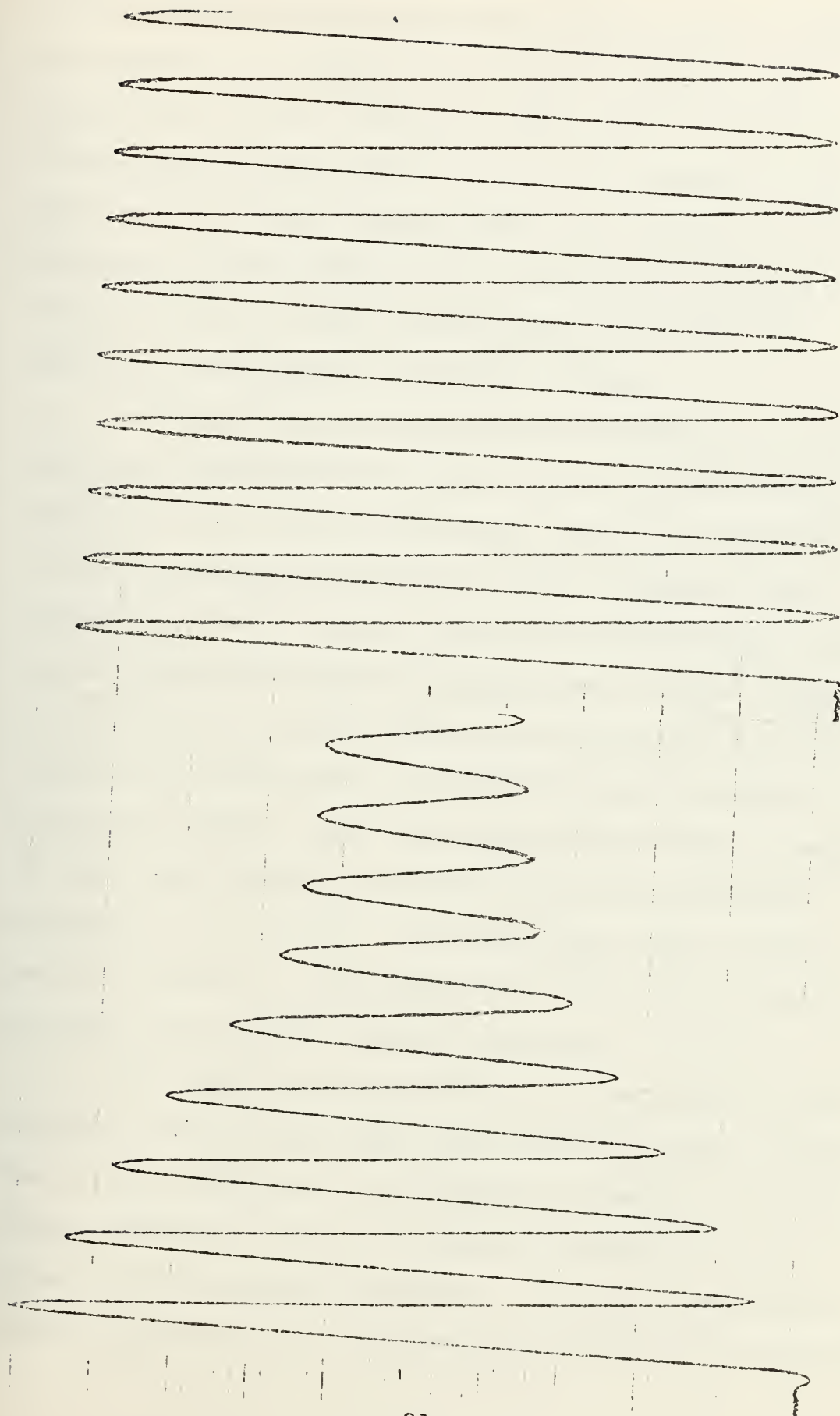
The amplitude change versus energy dissipation assumption is considered valid since it relates to the area contained by the stress-strain hysteresis loop of a material under uniform stress, i.e., a basic material property. This data also correlates well with logarithmic decrement data utilized in studies of anelastic materials [10].

B. ELECTRICAL RESISTIVITY MEASUREMENT

1. Resistivity as a Property

The measurement of electrical resistivity is a relatively common method used to identify the occurrence of phase changes in metals. Since it is a thermodynamic transport property, electrical resistivity is both a function of material composition and temperature.

When a material's lattice structure changes through a reordering process such as a phase change, the relative



(a)

(b)

FIGURE 4. Typical torsion-pendulum output: (a) high damping alloy, (b) low damping alloy.

atomic spacing between atoms may change, e.g., a cubic-to-tetragonal transformation. Also, changes in the lattice position of like and unlike atoms by substitutional diffusion may affect interatomic spacing. These types of structural changes affect the mobility of free electrons due to changes in the interatomic distances through which the free electrons must pass when the metal is conducting an electrical current.

Reordering processes may be considered to be of two types differentiated by the scale on which the reordering occurs. The "long-range" order of a material refers to the crystallographic order throughout the material, grain or crystal; while the "short-range" order may be considered as more localized such as the ordering of atoms around nuclei, embryo's, dislocations or grain-boundary discontinuities. In materials that contain different elements, the long-range ordered state consists of like atoms occupying specific symmetric positions throughout the lattice. The short-range order of the lattice consists of atom groups or unit cells in which the like atoms occupy regular positions.

The electrical-resistivity of a material is most sensitive to its long-range order, which directly affects the lattice structure in its magnetic domains, and of the domain structure itself. A domain consists of a group of atoms with like magnetic moments. An atom's net magnetic moment is determined by the spin direction of its electrons

which is affected by its electrostatic interaction with neighboring atoms (a function of lattice order, inter-atomic spacing, relative atom size, etc.). Materials are defined as antiferromagnetic if their atoms align themselves with opposite magnetic moments. Alloys of this type may still possess some degree of magnetism, depending on the relative magnitude of the magnetism of their unlike constituent atoms. Increasing the temperature of the alloy affects its resistivity by causing its long-range order to change (become disordered). In antiferromagnetic materials, the temperature at which the long-range order completely changes is called the Neel temperature (T_N) and is marked by a significant change in the material's magnetic resistivity.

The total resistivity of a material may be considered to be a combination of the resistivity of several sources. Analytically it can be approximated by the following relation [11] :

$$\rho = \rho_T + \rho_I + \rho_M \quad (7)$$

where ρ_T is the thermal resistivity, ρ_I is the resistivity due to impurities, and ρ_M is the magnetic resistivity. The impurity resistivity is generally constant and not a function of temperature. Magnetic resistivity varies with temperature as discussed above. The thermal coefficient of resistivity is a linear function of temperature.

The relative freedom of electrons varies significantly between different elements and markedly affects their resistivity's temperature dependence. Most metals are relatively good conductors at low temperatures, but as their temperatures are increased their conductivity decreases. This is generally a linear relation, and is primarily due to the increased thermal-vibration energy associated with the atoms in the lattice. As the amplitudes of the atomic vibrations increase the inter-atomic spacing is correspondingly reduced, thus making it more difficult for electrons to pass through the lattice.

There are certain metals, however, which exhibit an increased electrical conductivity with increased temperature. This is very common with the so-called intrinsic semiconductors. At ambient temperatures these materials generally possess a high resistivity due to the small relative number of free electrons available in each atom's conduction band. However, with increased temperature, these atoms become thermally excited and some of the electrons in the lower atomic levels gain sufficient energy to jump into the conduction band and increase the supply of electrons available to conduct an electrical current.

The resistivity behavior of an alloy will often vary considerably from that of a pure metal, particularly if the alloy consists of more than two metals. This behavior is often very complex depending on the number

of different phases and intermetallic compounds that the alloy forms. Since each phase and intermetallic compound has its own individual electrical characteristics, the overall electrical resistivity of the material is correspondingly affected by the amount and complexity of the alloy's structure.

The materials resistivity is affected differently by the type of phase change that occur. As previously described, during the aging treatment of Incramute, a time-dependent diffusion reaction occurs in which new phases form through a nucleation and growth process from a nonequilibrium parent phase. These processes occur at specific rates, each governed by an Arrhenius relationship as discussed previously. The change in resistivity associated with those phase changes will correspondingly be rate related.

The second type of reaction which occurs during heat treatment of Incramute is one associated with the quenching process. This is the cubic-to-tetragonal transformation associated with the formation of martensite discussed previously. The resistivity change associated with this reaction will depend on the amount of the matrix that transforms, and the relative difference in resistivity between the original matrix and the new martensitic phase.

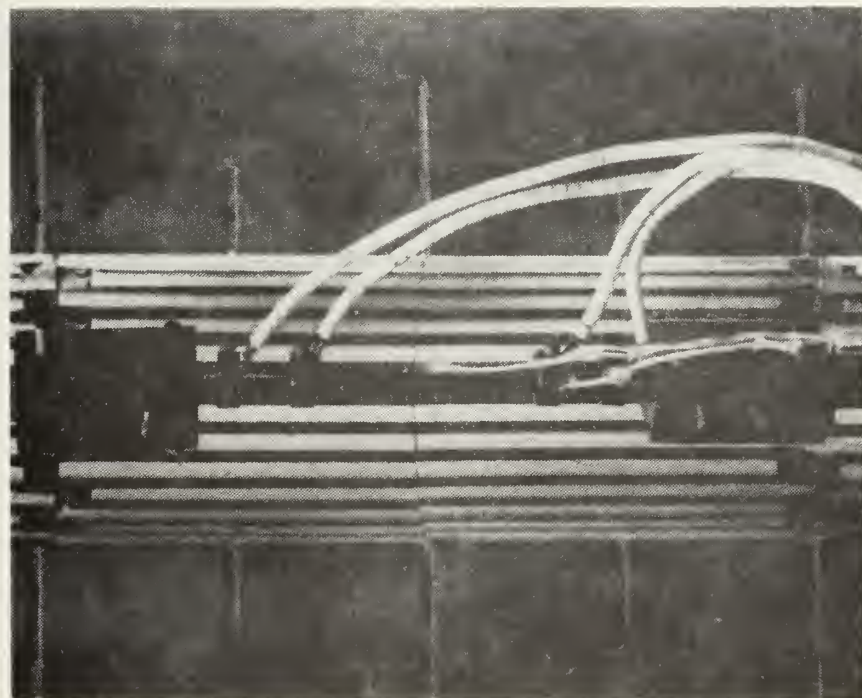
Because the resistivity behavior of any particular alloy is so complex; it is usually insufficient information on which to base the analysis of a material's structural

changes. However, when combined with information gained from other sources, a study of resistivity changes can make a very valuable contribution to the understanding of a material's thermodynamic behavior.

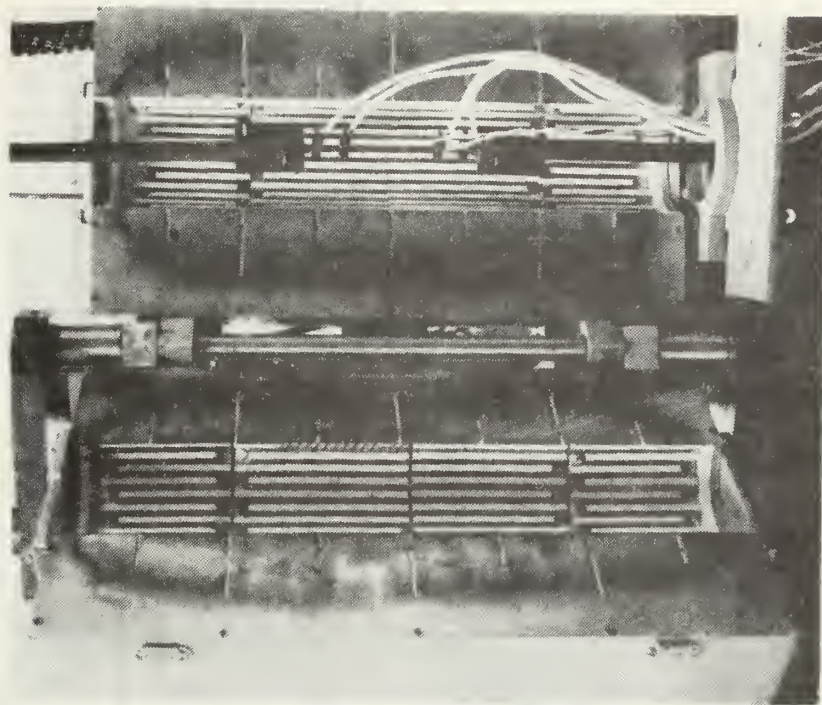
2. Resistivity Measurement

The method employed to measure specimen resistance utilized a Kelvin double bridge. The basic advantage of this type of bridge over others is that contact and lead wire resistances are automatically balanced out, resulting in an extremely sensitive resistance measuring capability. This results from utilizing four specimen contacts, two for current and two for voltage, with lead wires of the same lengths. The specimen connections are shown in Figure 5, and a schematic of the system and photograph are shown in Figures 6 and 3a respectively.

With the bridge in balance, the specimen resistance was read directly off the sliding contact scale. Initial and final bridge balance was obtained by first making a coarse balance on the null indicator, using the rotary and step resistors, and then making a fine adjustment on the calibrated slide resistance to null the galvanometer. Any subsequent bridge imbalance, caused by a change in specimen resistance, was then manifested by a millivolt signal to the chart recorder. Thus, by recording the specimen resistance at the beginning and end of the test, and using the chart recorder output, a continuous resistance record of the specimen was obtained throughout



(a)



(b)

FIGURE 5. Specimen connections for electrical resistivity test, (a) close-up of experimental device (b) specimen position in heater.

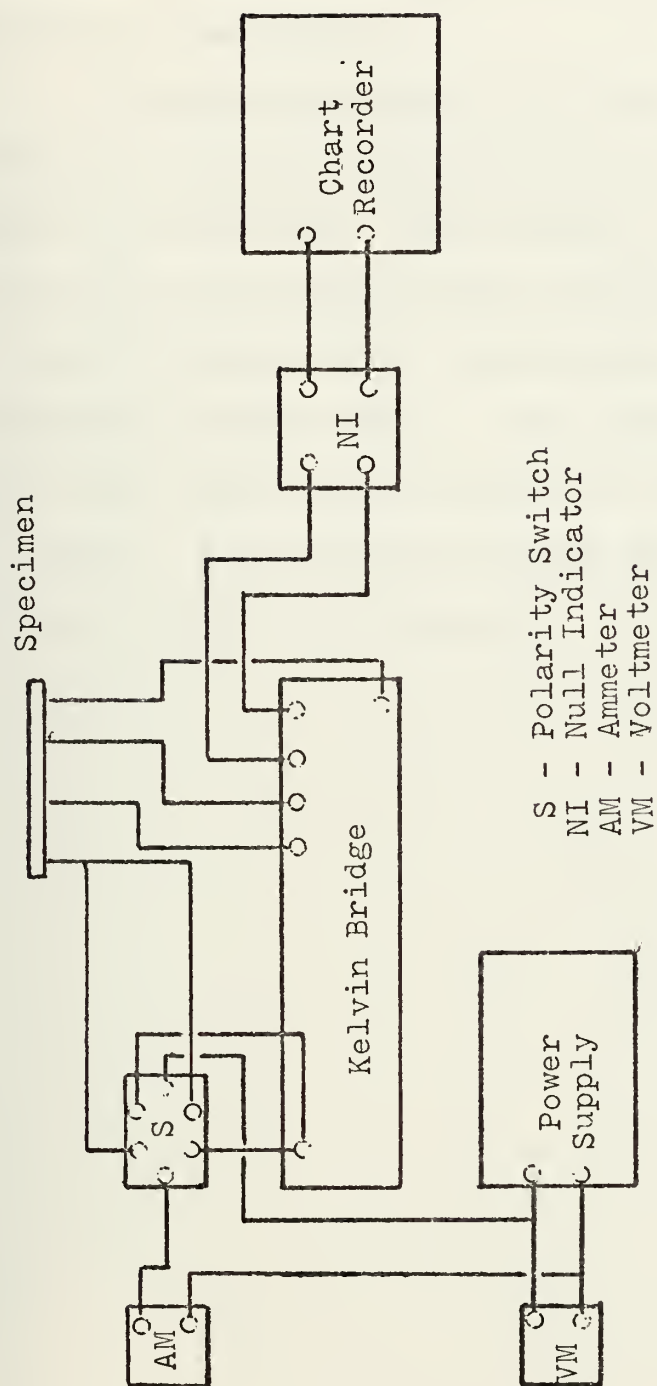


FIGURE 6. Schematic arrangement of resistivity measurement apparatus.

aging and quenching tests. The specimen temperature was also recorded simultaneously on the same chart so that resistivity versus temperature variation with time was continuously monitored.

A reverse polarity switch was used to ensure that contact and thermal resistances did not vary on different sides of the circuit. The accuracy of the system was checked by testing an annealed, 99.999% pure copper rod of similar dimensions to the Incramute specimens over a heating and cooling cycle. The resistivity values obtained were found to be within 7% of the handbook values for copper. A dimensioned drawing and photograph of the specimen are shown in Figure 7.

(a)

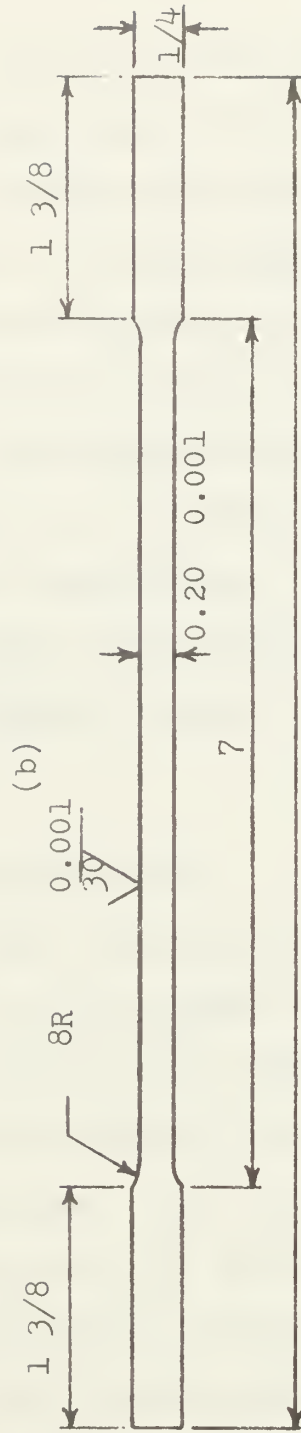


FIGURE 7. Test specimen for SDC and resistivity tests, (a) photograph (b) drawing.

IV. RESULTS AND DISCUSSION

The analysis of test results and data will be covered in five parts. The first three parts will cover the SDC-resistivity relationship, results concerning aging, and those that concern quenching. For both aging and quenching, the time-temperature kinetics affecting the SDC of Incramute will be discussed, followed by an analysis concerning the effects of tensile stress. The fourth section will relate the effect of stress during heat treatment of Incramute to the resulting SDC at room temperature. The fifth section will explain a phenomenological model which was developed to describe the effect of applied tensile stress on the SDC properties of Incramute.

A. CORRELATION OF SDC AND RESISTIVITY

Basic to this research was the requirement that specimen resistivity be correlatable with specimen SDC. This assumption was confirmed by plotting the change in the room temperature resistivity of the specimen for various aging conditions as shown in Figure 8a. The room temperature resistivity is the resistivity of the specimen after it has been cooled to room temperature (approximately 22°C) from its particular aging and quenching heat treatment. Note that the maximum change in specimen resistivity occurs at 425°C. For higher or lower aging temperatures, the change in specimen resistivity is less.

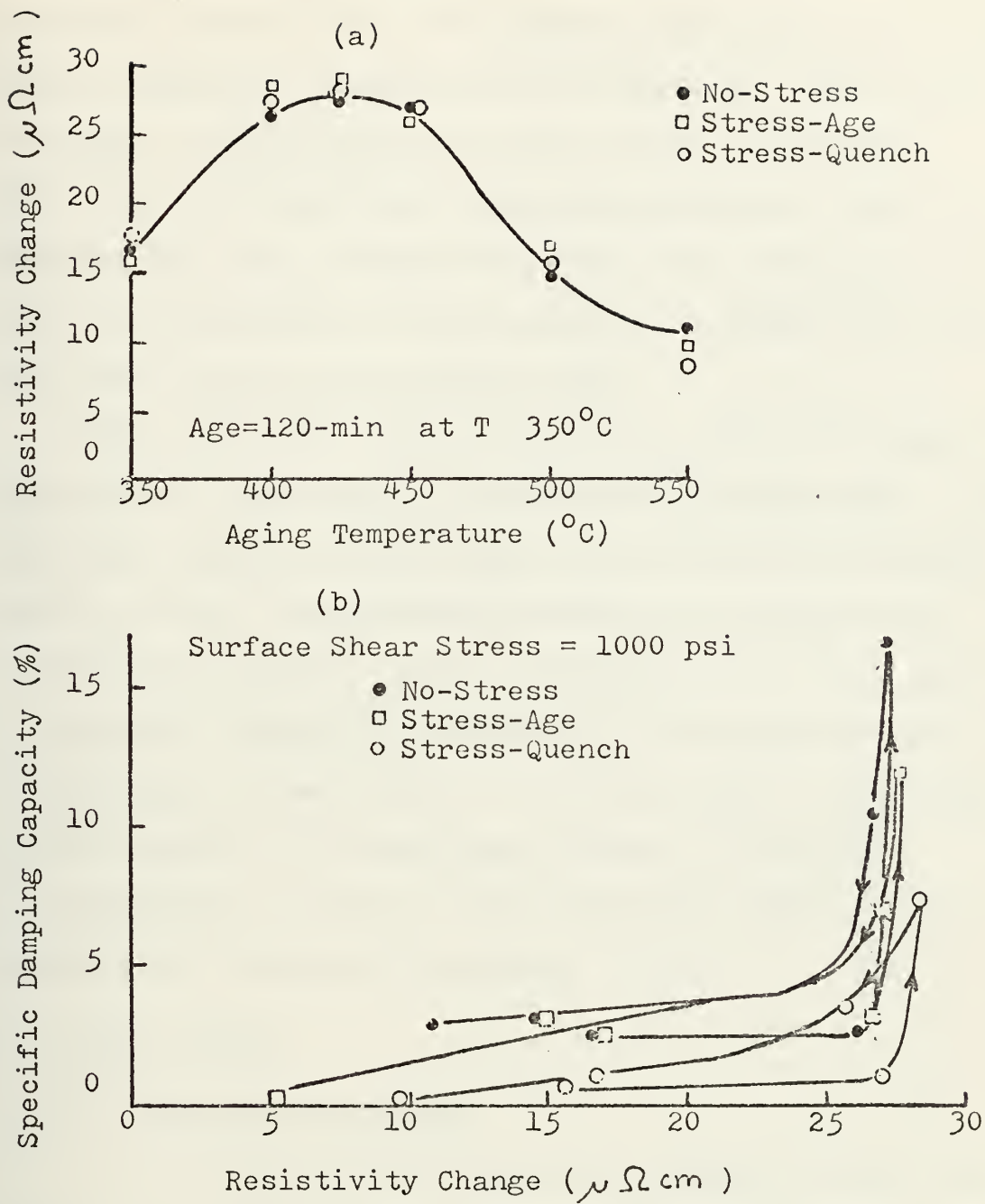


FIGURE 8. (a) Change in room-temperature resistivity for various aging conditions (b) SDC versus changes in room temperature from various aging conditions. The direction of the arrow denotes increasing aging temperature (Incramate I).

This maximum in resistivity change corresponds to a relative minimum on the room temperature resistivity versus aging temperature curves shown in Figure 9a. The curves of Figure 8 were derived from the curves of Figure 9. This resistivity minimum corresponds precisely with the maximum SDC value of Figure 9b which also occurs at 425°C. This correspondence is also indicated in Figure 8b by the very sharp peaks of the three curves.

These SDC plots, Figures 8b and 9b, are of SDC test data given by the 1000 psi surface shear stress test. Tests involving higher surface shear stress tests did not give such a precise correspondence between room temperature resistivity and SDC as shown in Figures 8 (c and d) and 9 (c and d). These differences will be discussed under surface shear stress effects. The low shear stress correlation, however, is significant, since it provides a valid indicator of SDC for ship silencing purposes (generally a low stress environment).

B. AGING PROCESS

1. Temperature Effects

An examination of Figures 10 through 15, raw data curves, gives some insight into why the resistivity minimum occurs in Figure 9a. Observe that the 425°C aging temperature curve (Figure 12) results in the lowest resistivity values at the end of the aging process. This corresponds to a matrix structure conditioned to give the best damping capability as evidenced by the 425°C SDC peak shown in

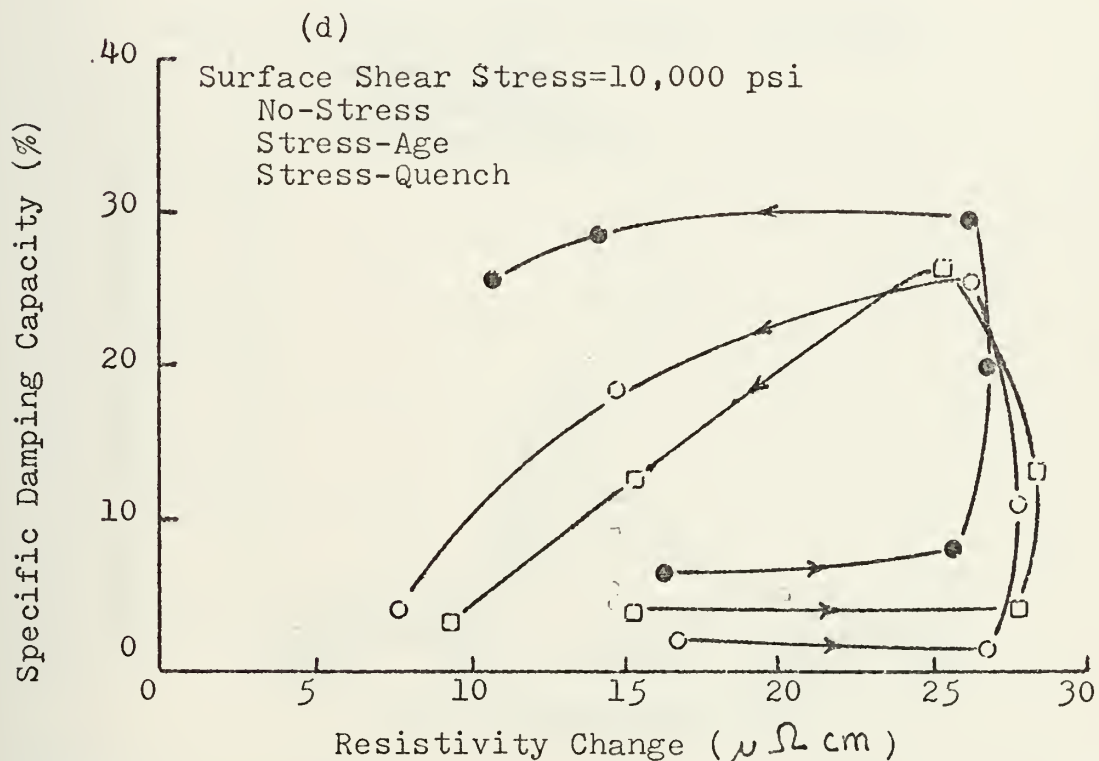
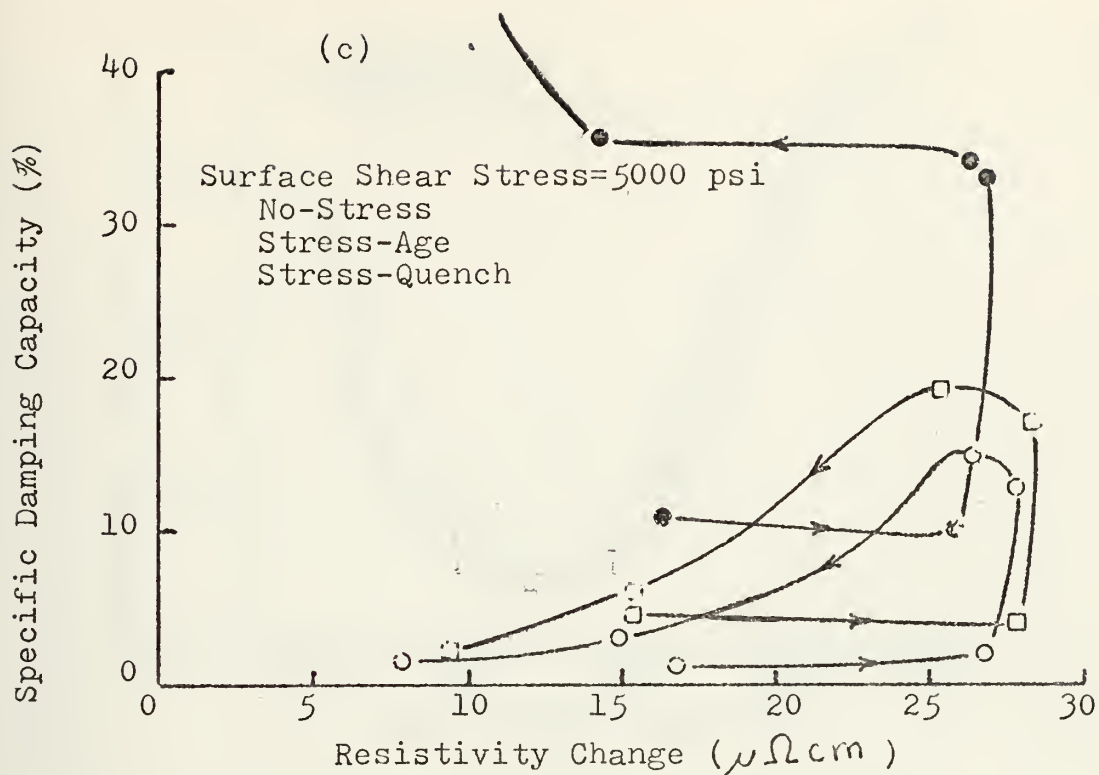


FIGURE 8. SDC at ambient temperature versus change in room temperature resistivity caused by heat treatment (c) SDC as measured by 5ksi surface shear stress (d) SDC as measured by 10 ksi surface shear stress.

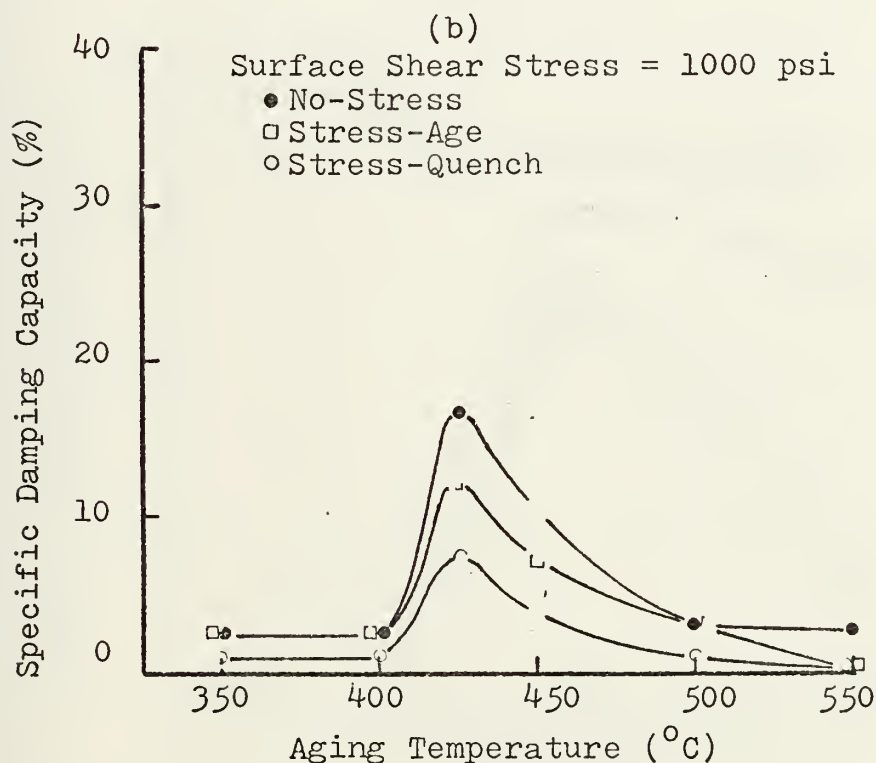
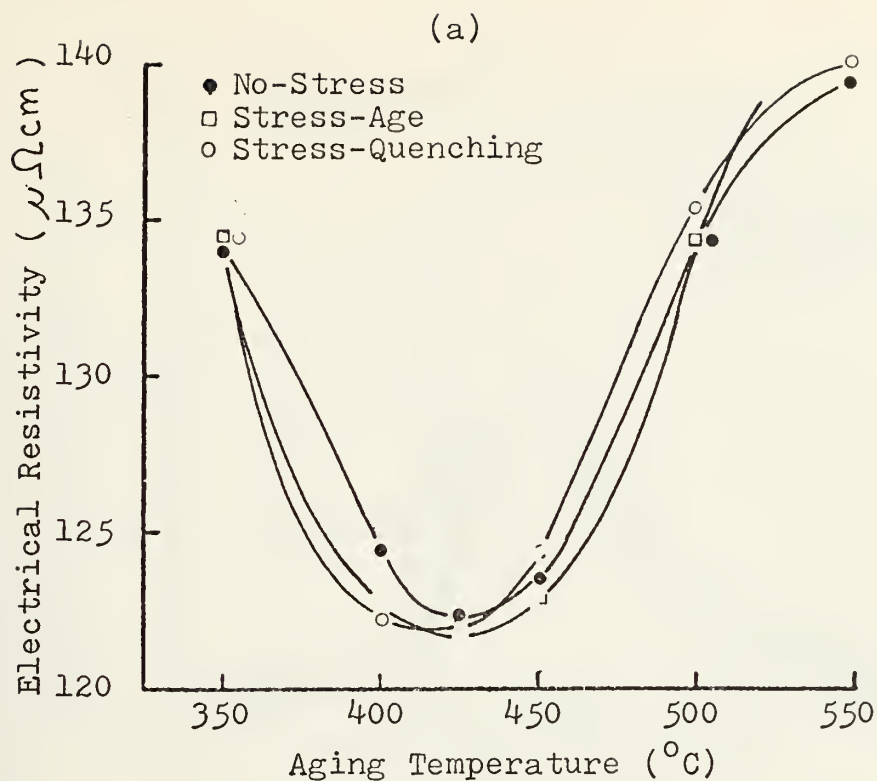


FIGURE 9. (a) SDC related to the room temperature electrical resistivity measured after heat treatment (Incrumute I, $t_{\text{Age}} = 120\text{-min}$ at $T = 350^{\circ}\text{C}$). (b) SDC versus aging temperature for various aging treatments as measured by 1 ksi surface shear stress.

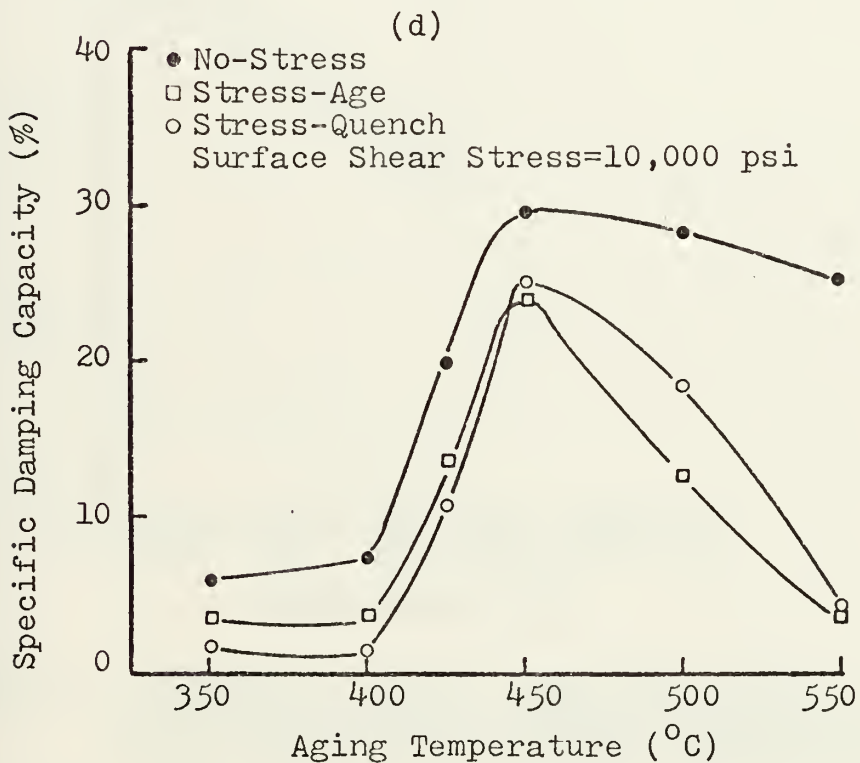
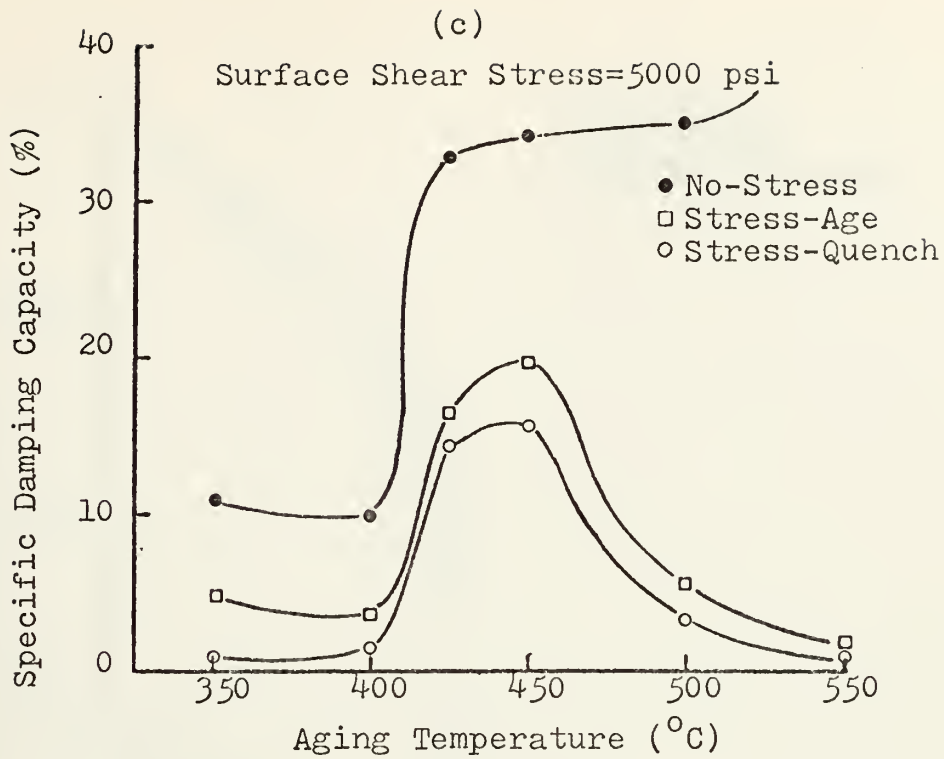


FIGURE 9. SDC at ambient temperature versus change in room temperature resistivity caused by heat treatments as measured by 1 ksi surface shear stress (Incrumute I, $t_{\text{Age}}=120$ -min at T 350°C).

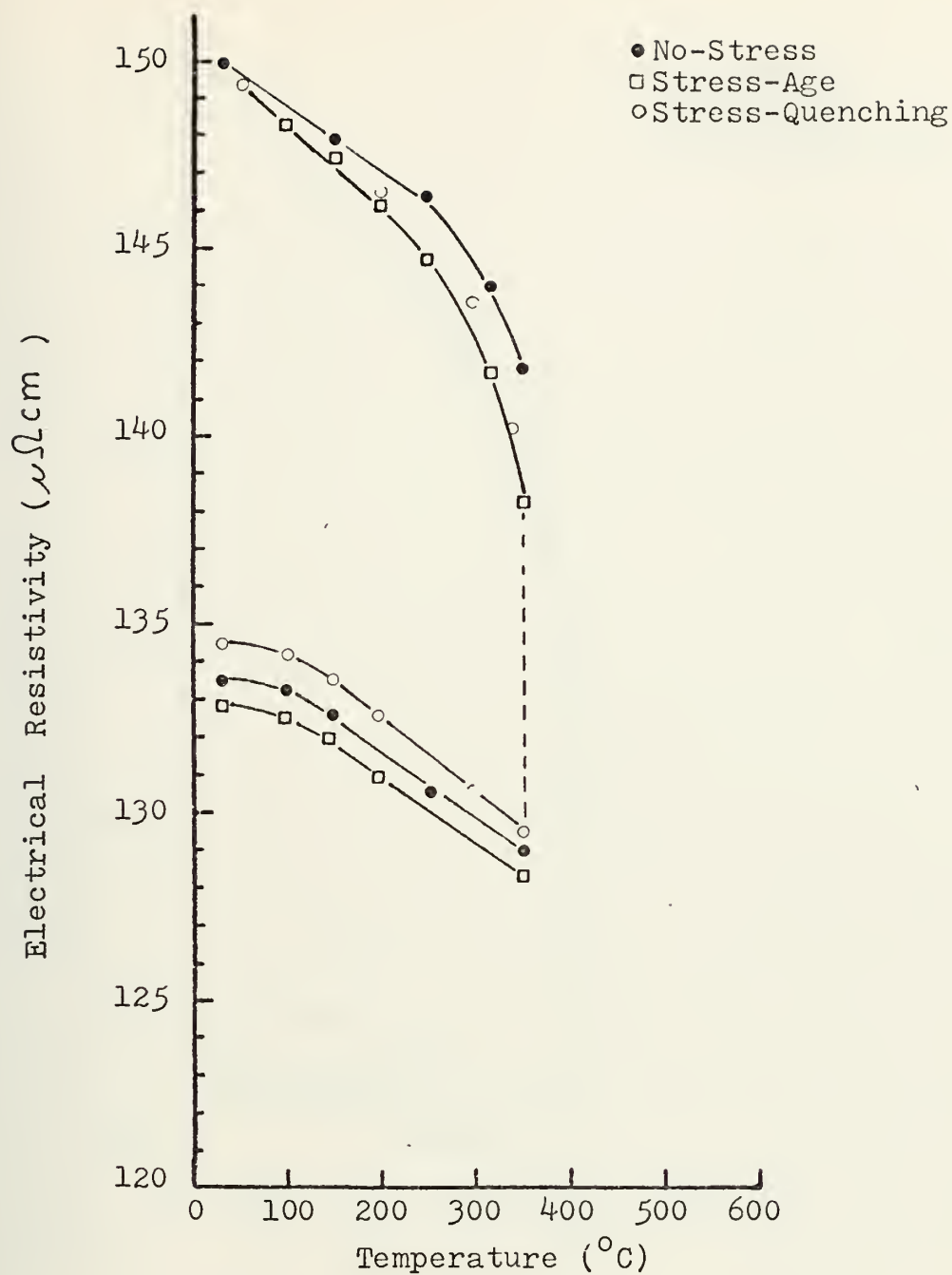


FIGURE 10. Resistivity versus temperature during aging and cooling under various loading conditions ($T_{\text{Age}} = 120$ min at $T = 350^{\circ}\text{C}$, Incramute I).

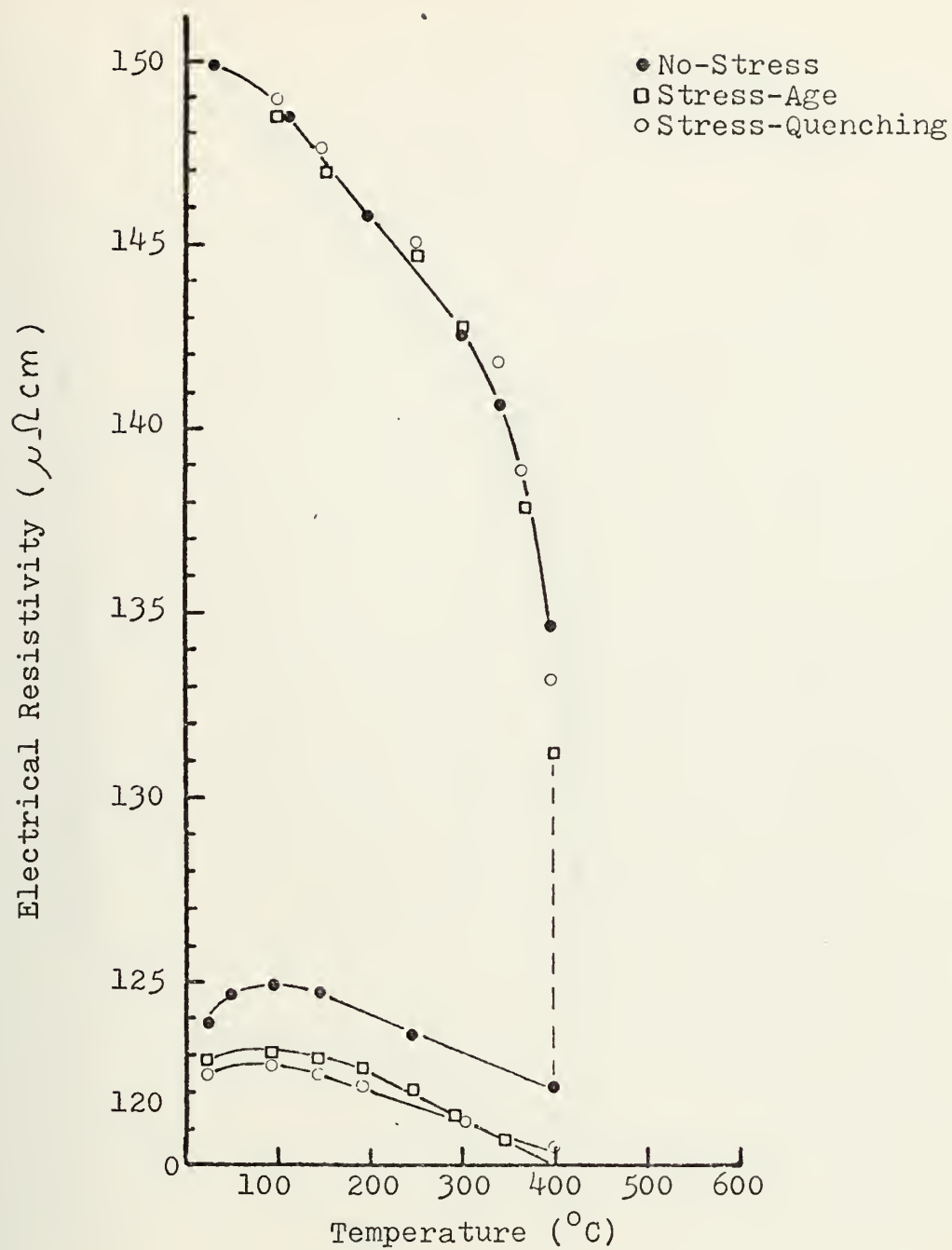


FIGURE 11. Resistivity versus temperature during aging and cooling under various loading conditions ($T_{\text{Age}} = 120 \text{ min at } T \ 350^{\circ}\text{C}$, Incramute I).

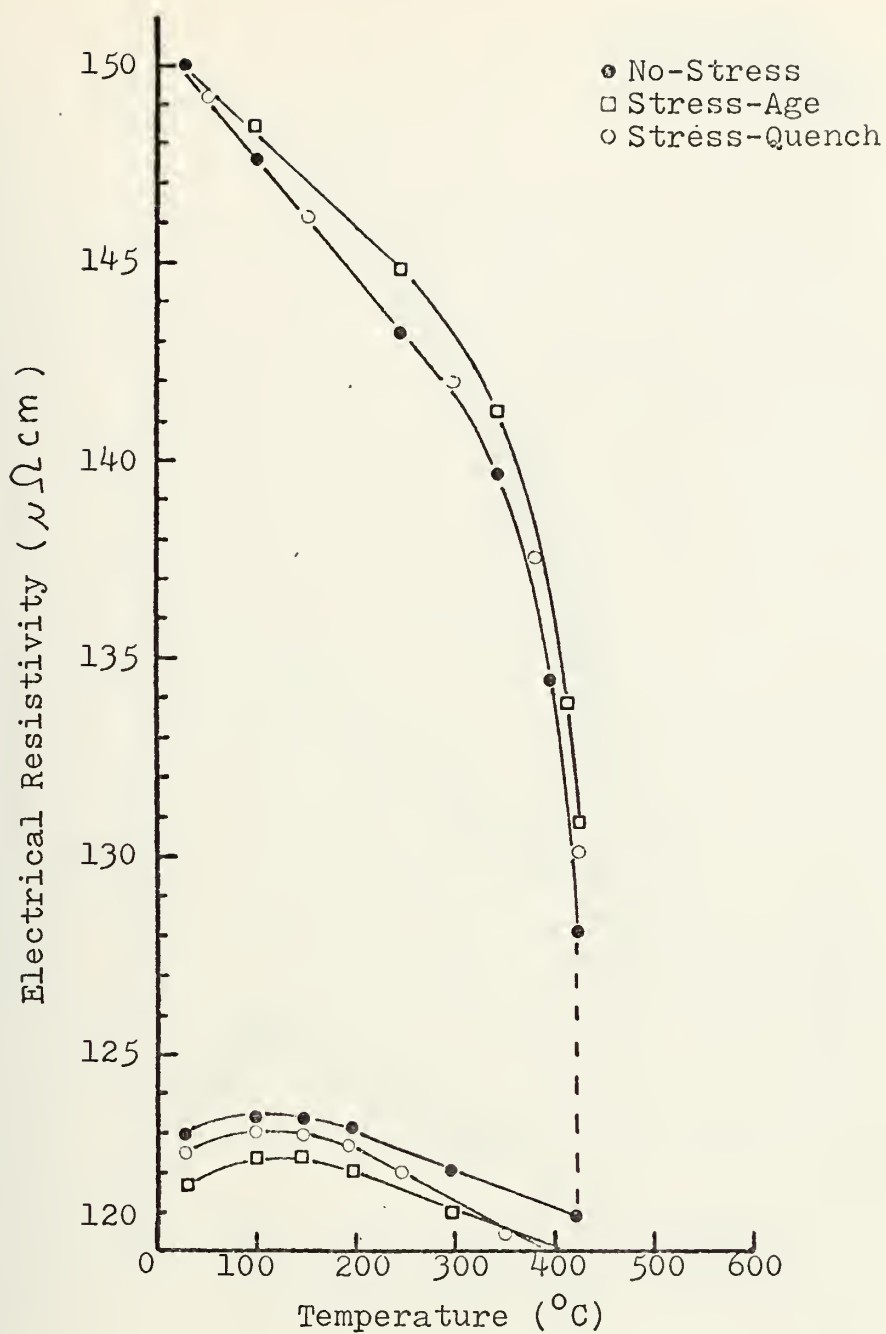


FIGURE 12. Resistivity versus temperature for aging and cooling under various loading conditions ($T_{\text{Age}} = 120$ min at $T = 350^{\circ}\text{C}$, Inframute I).

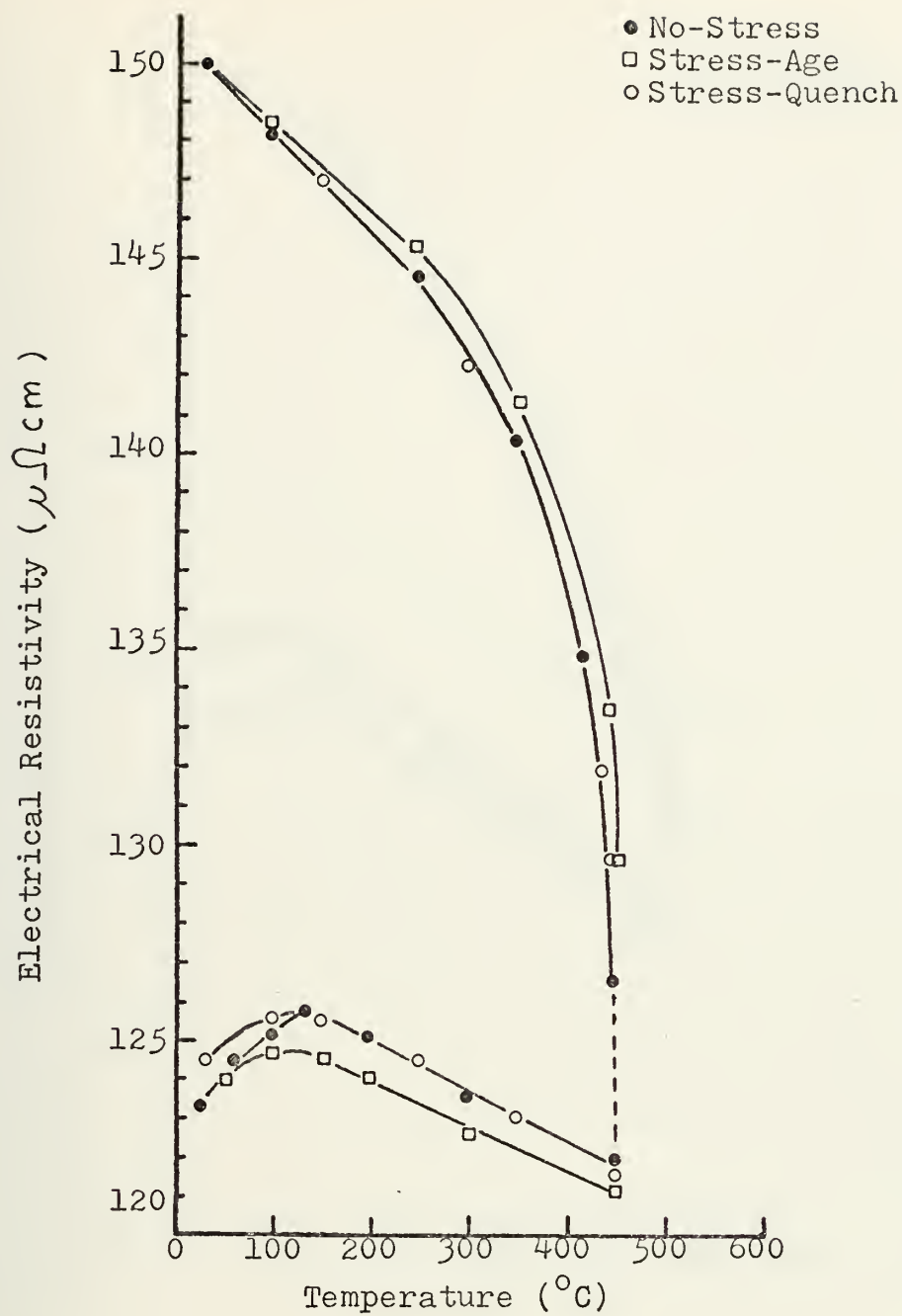


FIGURE 13. Resistivity versus temperature for aging and cooling under various loading conditions ($T_{\text{Age}} = 120$ min at $T = 350^{\circ}\text{C}$, Incramute I).



FIGURE 14. Resistivity versus temperature for aging and cooling under various loading conditions ($T_{\text{Age}} = 120$ min at $T = 350^{\circ}\text{C}$, Incramute I).

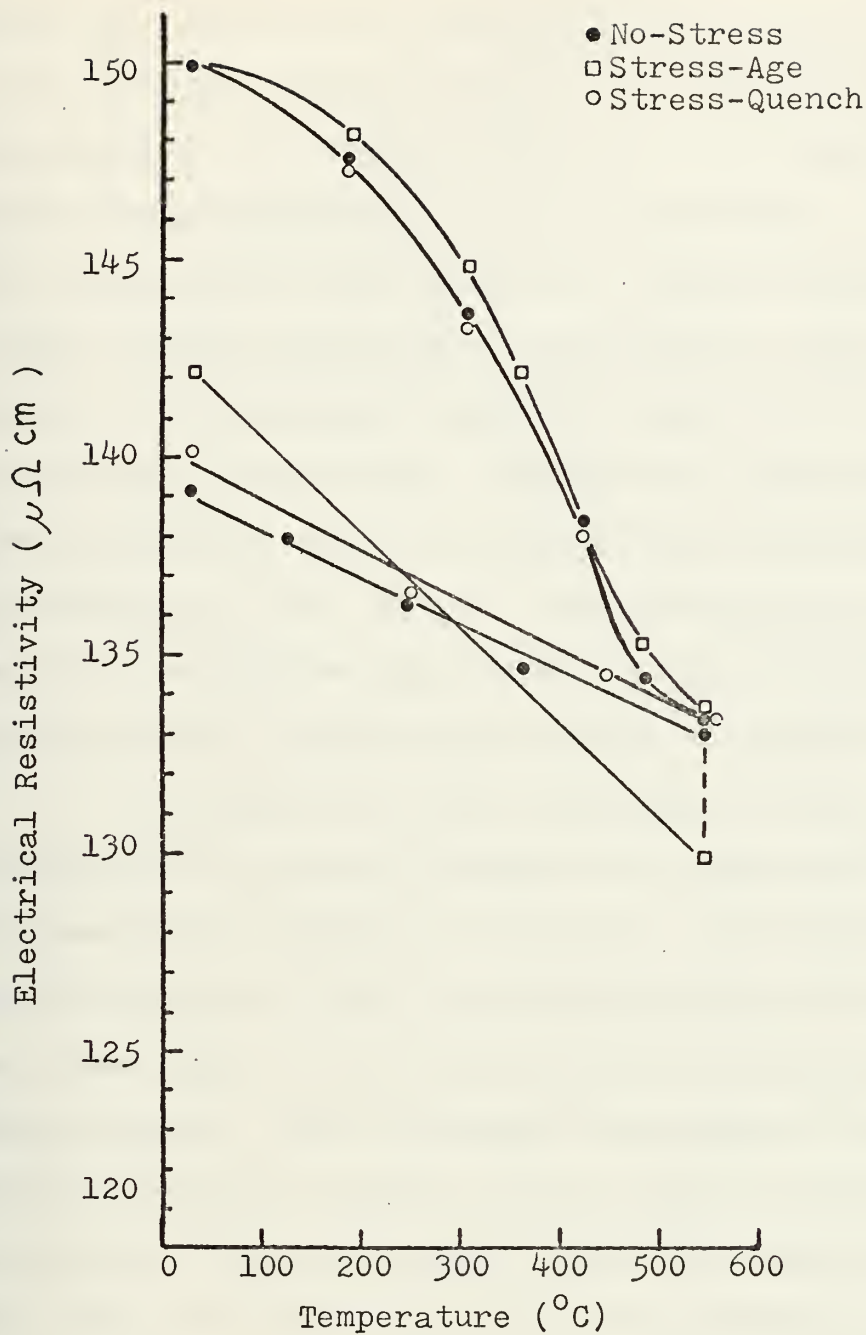


FIGURE 15. Resistivity versus temperature during aging and cooling under various loading conditons ($T_{\text{Age}} = 120 \text{ min}$ at $T \ 350^{\circ}\text{C}$, Incramute I).

Figure 9b. Note also, the significant turnover in the cooling (lower) curves of Figure 12. These inflections correspond to the initial formation of martensite, which results in a matrix with a lower resistivity. Unfortunately, the resistivity of the martensitic phase is very close to that of the parent phase, resulting in only a small change in the specimen resistivity curve with the formation of martensite on cooling. Consequently, the amount of martensite which forms on cooling cannot be deduced from the resistivity data alone. This insensitivity to the amount of martensite which forms is also evidenced by the very narrow resistivity band for the peaks of Figure 8b.

An indication of the mechanisms at work during aging process is given in Figure 16, which was derived from raw data in Figures 17 and 18. The intersection of the two slopes to form a concave downward plot indicates that some type of series process is occurring during the aging process. These processes correspond to two different activation energies, e.g., that of the line of least slope is approximately 5 kcal/mole and the activation energy for the steeper line is approximately 13.5 kcal/mole.

The 13.5 kcal/mole value is comparable to the activation energies for the most rapid of the diffusion processes in other metals. However the 5 kcal.mole value is extremely low to be attributed to diffusion of metal atoms, being more comparable to the diffusion

of atomic hydrogen in steel. To resolve the exact nature of these processes, x-ray or transmission electron microscope studies should be made.

2. Stress Effects

The stresses referred to in this section are those applied during the aging process (3% of the yield strength in tension). These should not be confused with the surface shear stresses developed during the damping tests or with the stress applied only during cooling from the aging treatment.

The effect of applied tensile stress during aging was determined from the data of Figures 17 and 18 and is shown in Figure 16. Figures 17 and 18 are the raw data aging curves for the material (Ingramite aged under no-stress and stress-age respectively). To plot each line in Figure 16 from these aging curves, the time required for the specimens to age to a specific resistivity value for all aging temperatures was used. The lower set of lines are for aging while under a tensile stress equal to 3% Y.S. Since these lines paralleled the upper, no-stress lines; but occur later in time, the activation energy is not stress dependent. Thus, it may be inferred that identical processes occur during the stress-age as in the age without stress, but the applied tensile stress retards the aging kinetics. The time delay is indicated by the vertical distance between corresponding points of constant resistivity for the same temperature. Note that

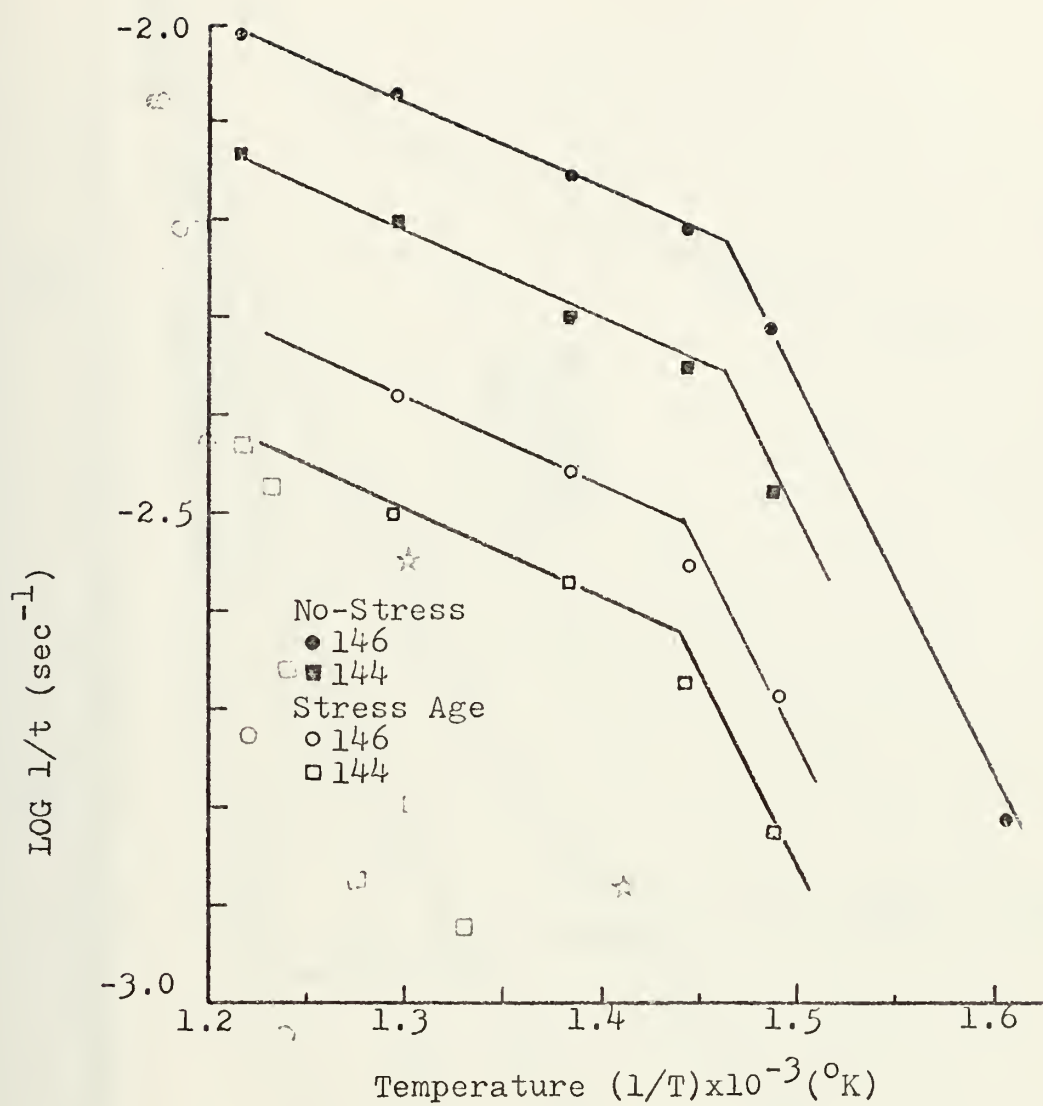


FIGURE 16. Time to constant resistivity versus aging temperature for no-stress and stress-age conditions. (Incramate I).

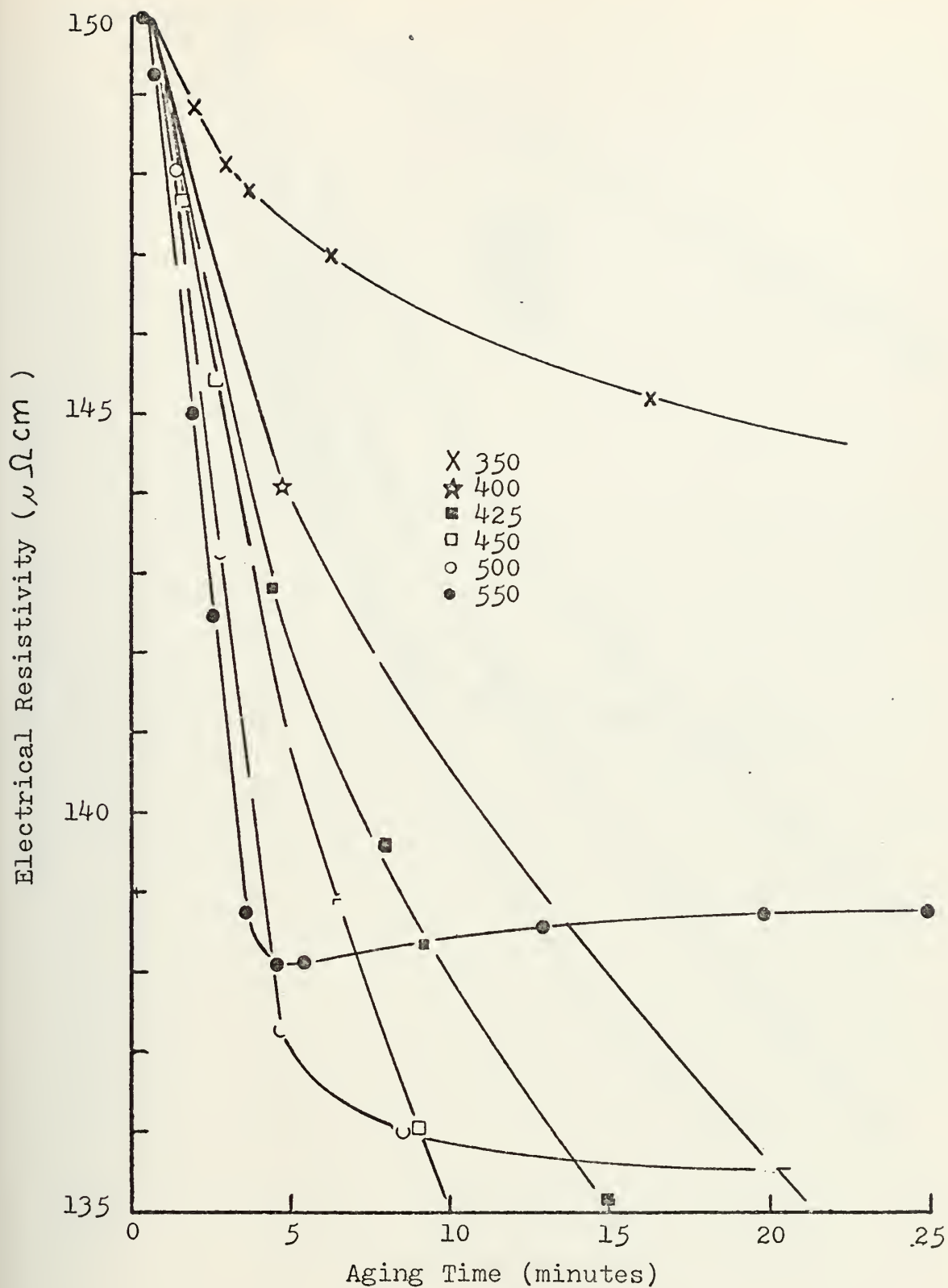


FIGURE 17. Resistivity versus aging time for various aging temperatures under no-stress conditions. (Incramate I).

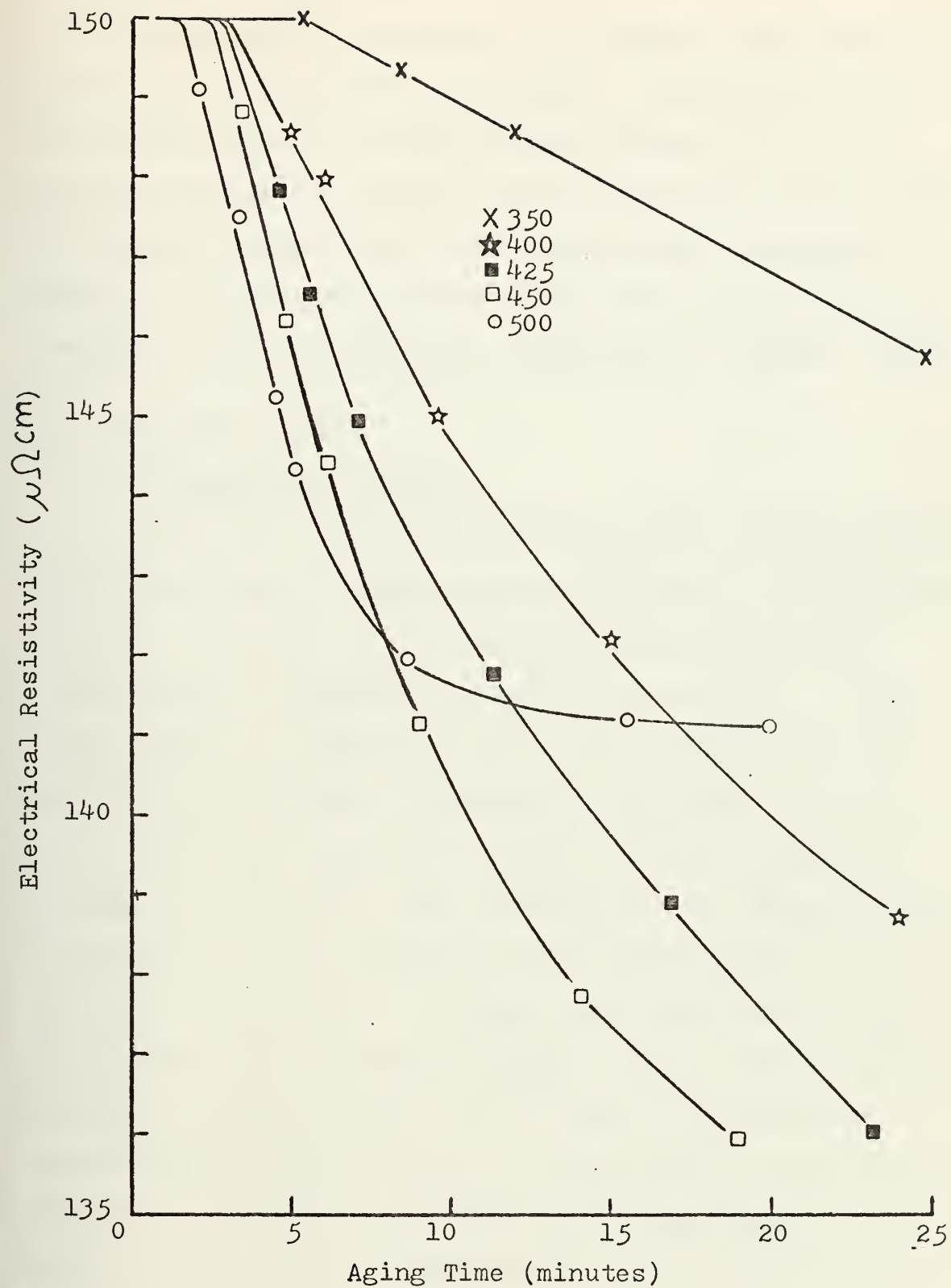


FIGURE 18. Resistivity versus aging time for various aging temperatures under 3% yield strength tensile stress conditions (Ingramute I).

since the lines are parallel, it is implied that this delay will be a constant depending on the magnitude of the stress applied during the aging process, e.g., the greater the applied stress, the more the aging process will be delayed. A practical cutoff point where the aging process is essentially prohibited, due to excessive stress, probably exists and should be identified by further testing.

C. QUENCHING PROCESS

1. Temperature Effects

The most important phenomena in the cooling process was the martensite transformation, critical to the SDC properties of Incramute. The parent-to-martensite phase transformation temperature shall be called T_{P-M} . It was found that T_{P-M} changed with both aging temperature and applied stress during both aging and colling.

To define T_{P-M} , the cooling curves of Figures 10 through 15 were used. This temperature was defined as the intersection of the tangents to both sides of the peak in the cooling curve. In theory, the temperature, T_{P-M} is a temperature between M_s and M_f . It was chosen because previous research showed that the type of martensitic transformation which occurs in Cu-Mn alloys is thermoelastic and not the burst-type martensitic transformation seen in steel [13]. Consequently changes in transport properties like resistivity are correspondingly gradual, and identifying the martensitic start temperature, M_s , as

the first deviation from the linear portion of the cooling curves was found to be experimentally inaccurate. It is assumed that T_{P-M} , as it has been defined, identifies a constant mixture of parent and martensite phases. Complementary testing with microscopy procedures were beyond the scope of this effort, but should be done to confirm these results.

Figure 19a illustrates how the aging temperature effects T_{P-M} . The maximum value of T_{P-M} occurs for the optimum low-stress damping condition (425°C) as seen by comparison with Figure 9. This correspondence is significant since it implies that the structure with the highest transformation temperature will have the best low-stress damping properties at room temperature. Figure 19a also indicates how stress, applied during aging, retards the aging processes and consequently lowers the transformation temperature. This effect is reflected consistently in all of the damping curves by the reduced stress-age SDC values, and implies that the total amount of martensite that forms in the stress-aged samples is less than that formed in the samples aged without stress.

2. Stress Effects

Figure 19a also shows the effects of applied stresses during the quenching process. T_{P-M} , for the optimum damping condition, is clearly lowered. This effect of the reduced T_{P-M} is correspondingly reflected in the SDC plots of Figures 8 and 9. The SDC values of the stress-quench

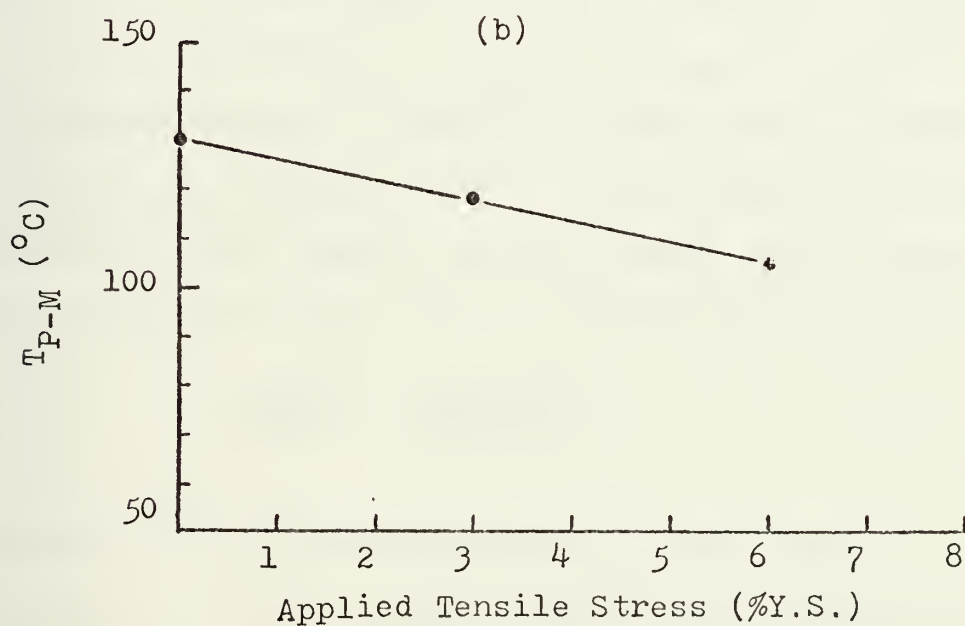
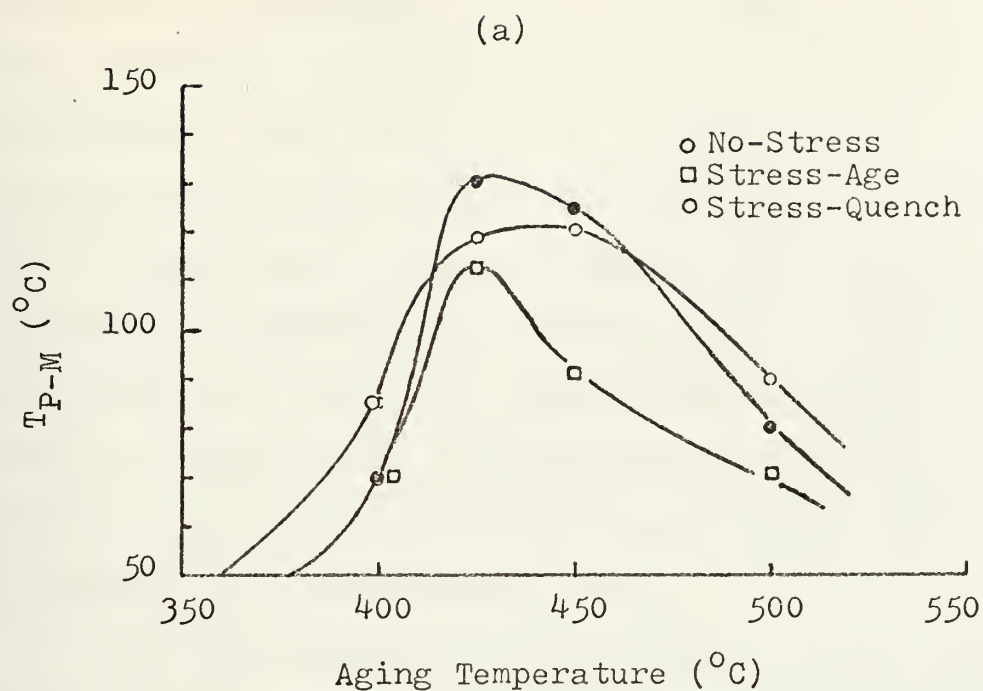


FIGURE 19. (a) Martensite start temperature versus aging temperature. (b) Martensitic transformation temperature versus applied tensile stress during quench (Incramate I).

specimens are generally below the SDC values of the no-stress specimens. Less martensite must form during the stress-quench than during the no-stress test, and transformation strains associated with the martensite which does form may prevent more martensite from forming after the stress is removed (at room temperature). Otherwise, in the absence of any such transformation strains, the removal of stress after quenching would permit the remainder of the martensite to form and result in the same SDC values as in the no-stress tests.

With an increase in the quenching stress to a value of 6% of the yield strength, a definite relationship was established between T_{P-M} and the applied tensile stress. This relationship is plotted in Figure 19b for specimens aged under no-stress at 425°C. The linear relationship between T_{P-M} and applied tensile stress during quenching may be correlated with the Clausius-Clapeyron equation [14] :

$$\frac{d\sigma^{P-M}}{dT} = \frac{\rho \Delta H^{P-M}}{\epsilon_L T_0} \quad (8)$$

where $d\sigma^{P-M}/dT$ is the reciprocal of the slope of the line in Figure 16b, ρ is the density, T_0 is the equilibrium transformation temperature ($\Delta G=0$), ΔH^{P-M} is the enthalpy of the transformation, and ϵ_L is the maximum realizable crystallographic strain developed by the transformation. Since three of these parameters, ϵ_L , T_0 , and ΔH^{P-M} are not known, only their ratio can be derived from the data accumulated. Thus, it was found that:

$$\frac{\Delta H^{P-M}}{T_0 \epsilon_L} = 397 \quad \text{in}/^\circ\text{C}$$

and the slope of the line in Figure 19b was found to be $-9.36 \text{ }^\circ\text{C}/1000 \text{ psi}$.

The relatively high slope of this curve indicates a very strong stress dependence. By comparison, Patel and Cohen found slopes of from 0.5 to 1.0 ($^\circ\text{C}/1000 \text{ psi}$) for various nickel steels [9]. The negative slope of this line indicates that the specific volume of the martensitic phase is less than the specific volume of the parent phase. It also suggests that for this material, the transformation strain component of equation (5) is related to a significant, negative volume change. Such a negative volume change would tend to oppose the always positive shear-work term and retard the transformation.

Because the martensitic transformation in this Cu-Mn alloy is so stress dependent, the hysteresis loop developed by such a transformation should be relatively wide (a Type II thermoelastic martensite). The hysteresis loop for the high stress case (tensile stress equal to the percent yield strength) is shown in Figure 20. The specimen was first aged at 425°C (no stress), forced-air quenched under stress to room temperature (22°C) and then reheated while still under stress to 200°C . After resolutionizing the specimen at 700°C for 40 minutes, the test was repeated except that the reheat was made without stress to get the dotted portion of the curve.

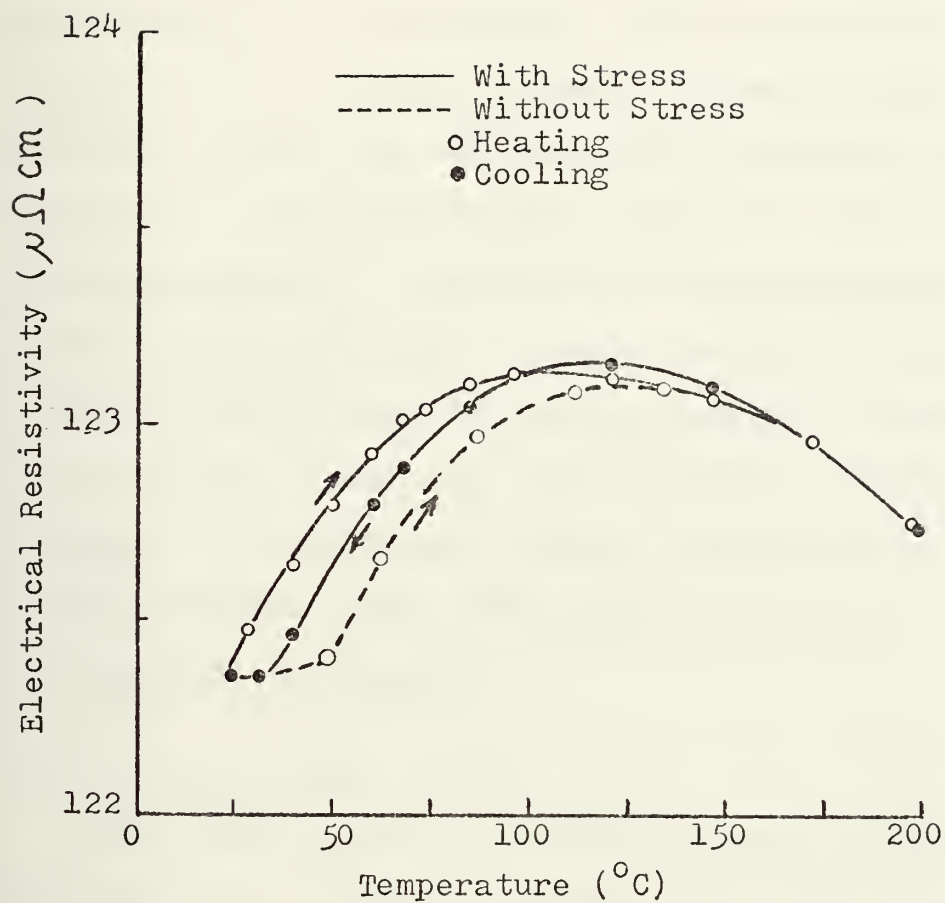


FIGURE 20. Resistivity versus temperature for 6% Y.S. tensile stress applied during air quench, with subsequent reheat to show hysteresis. Quench follows age at 425°C -120 min at T 350°C (Incramate I).

The behavior of the specimen under the stress-reheat (Figure 20) was not unexpected. This type of behavior has also been observed in Au-Cd alloys [11] and more recently in NiTi alloys [14]. This type of behavior is believed to be caused by a build-up of elastic lattice strains at the interface between the martensitic phases and parent matrix as the martensite platelets are born and grown. Residual stresses associated with these lattice strains are magnified by the applied stress. Thus, when the specimen is heated under stress, the martensitic plates begin to revert immediately because of the cumulative effect of the applied and residual elastic stresses. When reheated without external stress, the system reverts along a path similar to other thermoelastic, martensitic alloys.

D. SDC TEST-STRESS EFFECTS

Test results from the specific damping capacity tests are plotted in Figure 21, as raw data, and arranged according to the shear stress level of the damping test. The first observation to be made is that, for samples aged 120 minutes at 425°C, effect of tensile stress during either aging or cooling is to reduce the materials damping capacity across the entire spectrum of aging and cooling schemes. This effect has been examined using the resistivity data, but is mentioned here to emphasize the consistency between the two independent tests.

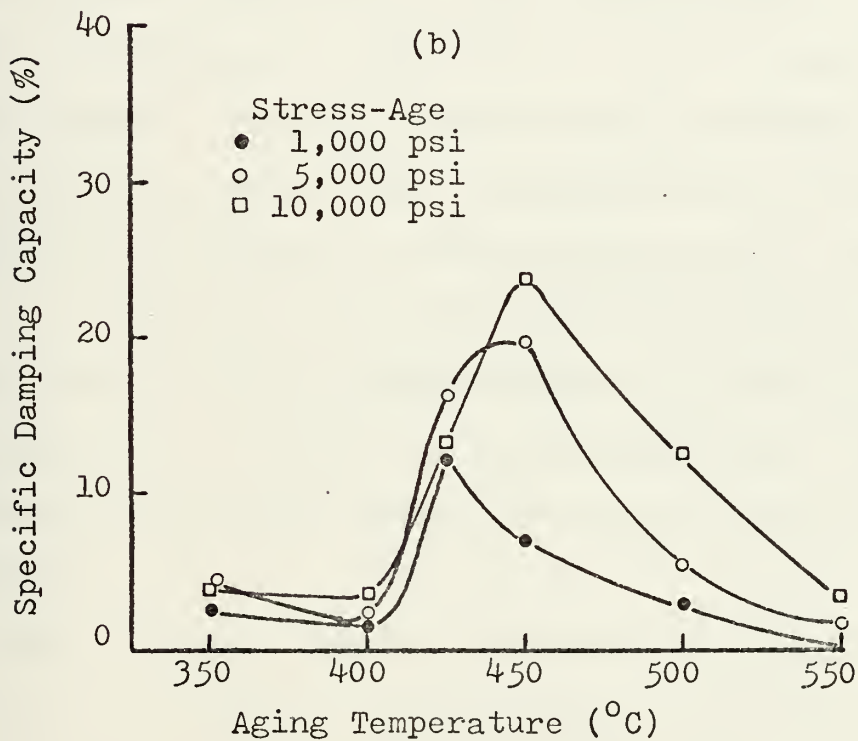
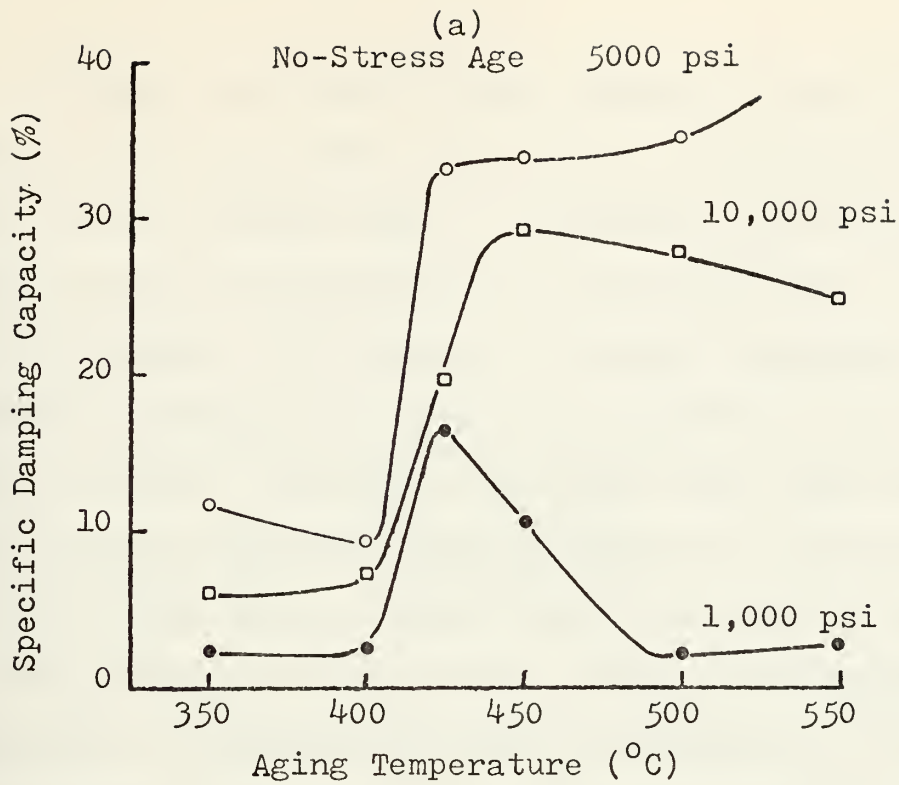


FIGURE 21. SDC versus aging temperature for various heat treatment conditions ($t_{\text{Age}}=120$ min at T 350 $^{\circ}\text{C}$, Incramute I). (a) No stress during age, (b) 3% Y.S. tensile stress applied during age.

To analyze the shear stress effects, it must be kept constantly in mind that this was the only parameter that was varied in the SDC Tests. Increasing the surface shear stress was accomplished by increasing the torque on the specimen. Increasing the torque corresponds to increasing the angle of twist, or amplitude of the induced free vibration. Generally, the tests were made immediately following the specimen's heat treatment by successively increasing the surface shear stress for each SDC Test.

The effect of surface shear stress on the damping properties of Incramute is shown in Figures 9, 21 and 22. The nonlinear character of this stress effect is most evident in Figure 22, where SDC is plotted against surface shear stress. This was only done for two aging temperatures, but could be done for all. However, all of the general effects are contained in Figure 22 and can be summarized as: (1) specimens aged without stress showed the most sensitivity to surface shear stress; (2) shear stress dependence is a function of aging temperature and time, stress applied during aging, and stress applied during quenching.

This nonlinear behavior obviously is directly related to the microstructure of the material, which is dependent on the material's history of heat treatment. It is postulated that the SDC is a strong function of the volume of thermoelastic martensite contained in the material, and that the amount of martensite in a specimen

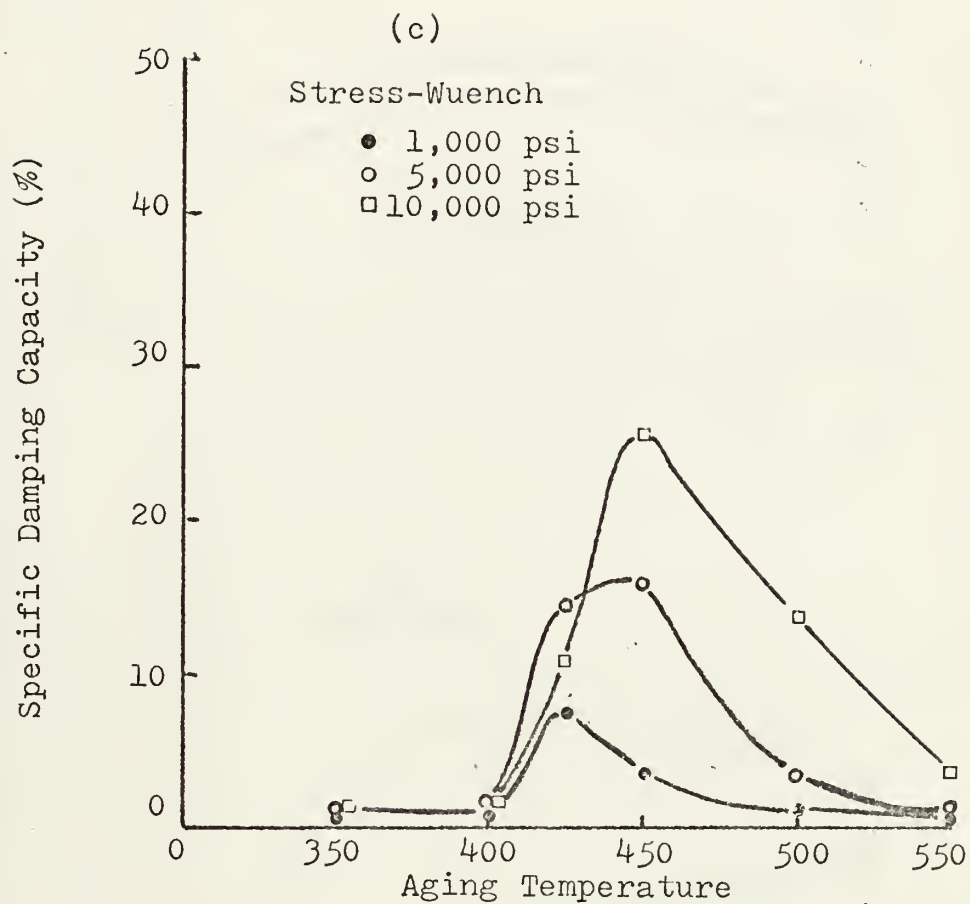


FIGURE 21. SDC versus aging temperature for 3% Y.S. tensile stress applied during quench.

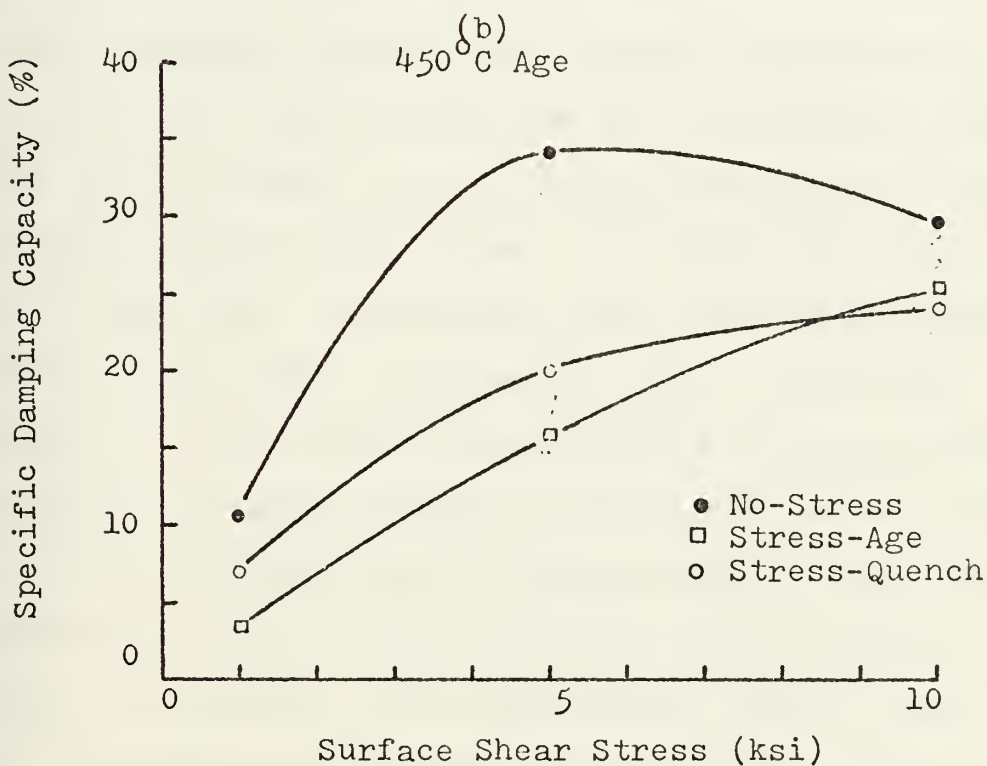
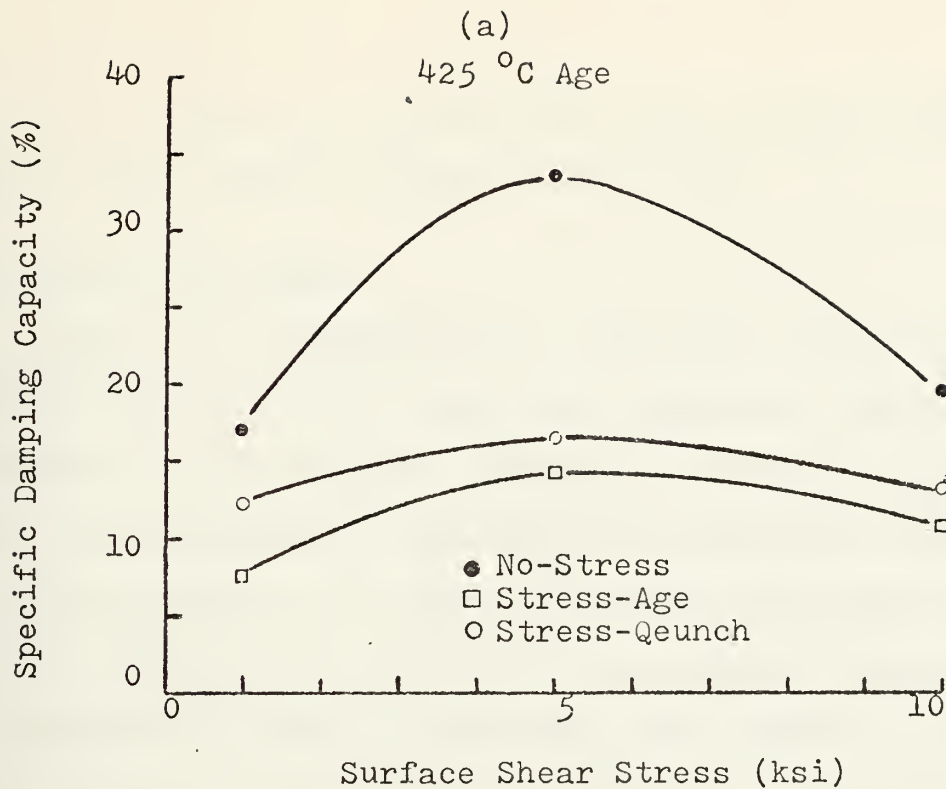


FIGURE 22. SDC versus surface shear stress for aging at
(a) 450°C (b) 450 °C ($t_{Age}=120$ min at
T 350 °C, (Incramate I).

is stress dependent, and may even depend on the initial shear stress applied during the SDC test.

E. BEHAVIORAL MODEL

Figure 23 is presented as a behavioral model which schematically describes the stress dependent, SDC characteristics of Incramute. Generally, Figure 23a states that the percentage of martensite in Incramute is dependent on stress present during heat treatment; and that, for the same shear stress during SDC measurement, the amount of martensite is less if the sample was stressed in tension during the age or during the quench. Figure 23B states that the maximum SDC occurs at some optimum volumetric amount of martensite.

The statements made by these curves correlate well with the experimental data accumulated by this research. Results of the heat treatment tests of this study indicate that:

(1) aging temperatures greater than 425°C (for 120-min aging times) cause a reduction in the material's damping capacity at low shear stresses but not at high shear stresses; (2) for samples heat-treated at time and temperatures which would normally produce maximum damping, the martensitic transformation temperature is significantly reduced by the application of tensile stress during either the age or the quench (see Figure 19b). Both of these facts, supported by SDC and resistivity data, indicate that the type of heat treatment and amount of applied

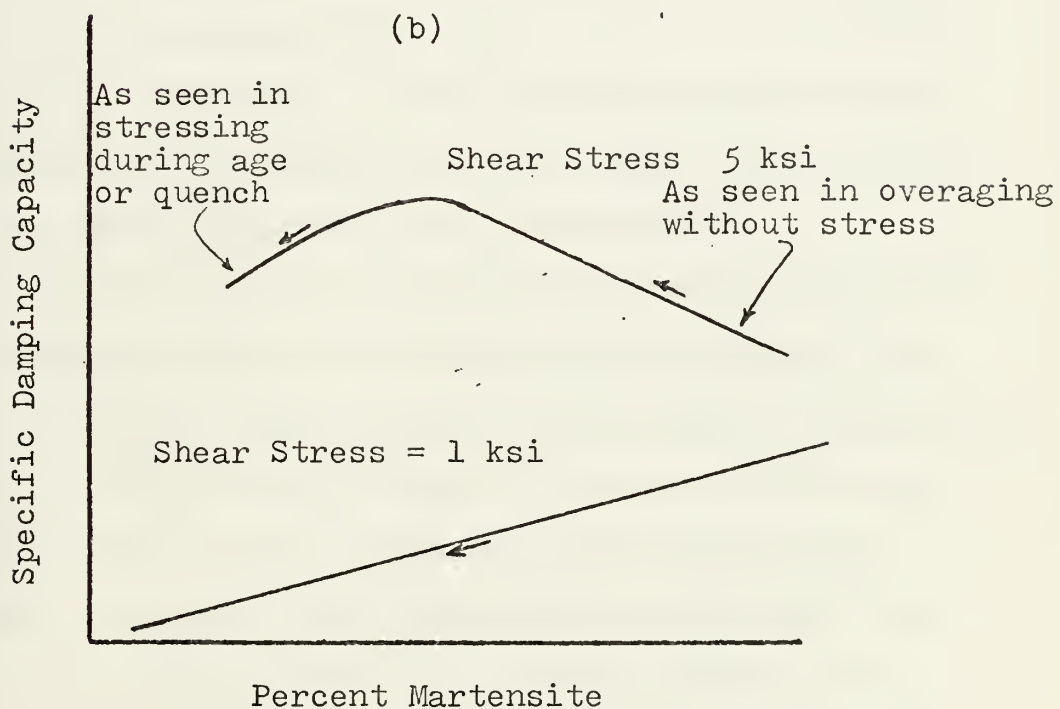
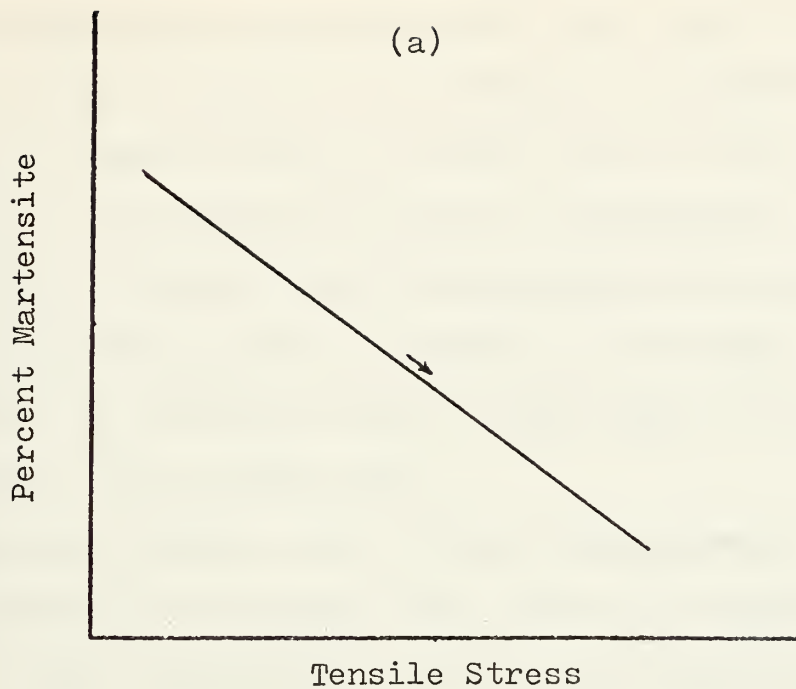


FIGURE 23. Microstructural model of the SDC of Inframute I.

stress during age and quench affect the amount of martensite that is formed in the material on quenching.

If the shear stress in the SDC test is low, SDC increases with increased percent of martensite, implying that the mobility of the intramartensite twin boundaries or intermartensite plate boundaries is the main damping mechanism at low shear stress. This affect is shown by the lower line in Figure 23b.

Applying surface shear stress levels greater than 5 ksi resulted in the highest SDC values for samples, which by all other indications, were not fully martensitic. Specifically, the highest SDC values (as measured by shear stresses greater than 5 ksi) occurred in overaged ($T_{Age} = 425^{\circ}C$) specimens. Yet, resistivity measurements gave transformation temperatures for these samples which were only about $30^{\circ}C$ above room temperature.

The possibility of high damping by parent-martensite phase boundary motion is further substantiated by the effect of tensile stress applied during aging or quenching. Figure 9c indicates this effect by showing a pronounced decrease in SDC for the stress-age and stress-quench specimens (overaged), which must contain even less martensite than the specimens aged without stress (which themselves are not fully martensitic, but are high damping). The upper line in Figure 23b summarizes the hypothesis of energy absorption at high shear stresses by interphase boundary motion in a format consistent with all observations.

The effect of overaging of SDC at high shear stresses is indicated by an arrow in Figure 23b, i.e., data indicates at optimum mixture of parent and martensite phases is needed for maximum high stress damping.

The effect of tensile stress applied during aging or quenching is indicated by the arrows on Figures 23a and 23b. The implication that less martensite forms in the samples aged under stress than in the samples aged without stress was deduced from consistent relationships between Figures 8, 9, 16, and 19. Figures 8 and 9 indicate that the SDC of the material is less for the specimens aged under stress than for the specimens aged without stress. Figure 16 shows that the aging kinetics are retarded by applied tensile stress. And, Figure 19 shows that the changes in aging kinetics are manifested in a reduced T_{P-M} . Reducing T_{P-M} reduces the temperature range ($T_{P-M} - T_{Room}$) over which the martensite forms. Thus, for M_f less than room temperature, less martensite would be formed in the stress-age samples, aged under stress, than in the samples aged without stress.

Although the stress-quench specimens were aged without stress, they too showed a reduced SDC. This is also attributed to less martensite being permitted to form (as previously discussed on page 53) and would also be indicated by the arrow on Figures 23a and 23b.

The nonlinear dependence of SDC on stress used to measure SDC (Figure 22) cannot be directly explained

by this model; primarily because, one cannot assume that uniaxial tension and torsional stresses have the same microstructural effects. It is interesting to note, however, that the data of Figure 22 are compatible with the assumption that initial torsional stress during SDC measurement has the same effect on this alloy as does uniaxial tension, i.e., that high stress decreases the percent martensite present. It is possible that high applied shear stresses cause a reduction in total parent-martensite boundary area, thereby reducing the measured SDC.

F. RESISTIVITY BEHAVIOR

Resistivity-temperature data were taken during heating of a specimen in an effort to determine the Neel temperature, T_N , of the material. Results are plotted in Figure 24. The inflection point in the M curve was labeled as T_N (approximately 763°K). However, the accuracy of this temperature is subject to several complicating factors which are mentioned here as a consideration for judging the data's accuracy.

The ternary alloy being measured is quite complex in it's behavior as seen in Figure 3. When heated from the solutionized and quenched condition, as this test sample was, the material is highly metastable and begins to age relatively quickly for temperatures above 300°C. This aging process consists of compositional changes which affect the material's antiferromagnetic ordering process, and subsequently, the material's resistivity.

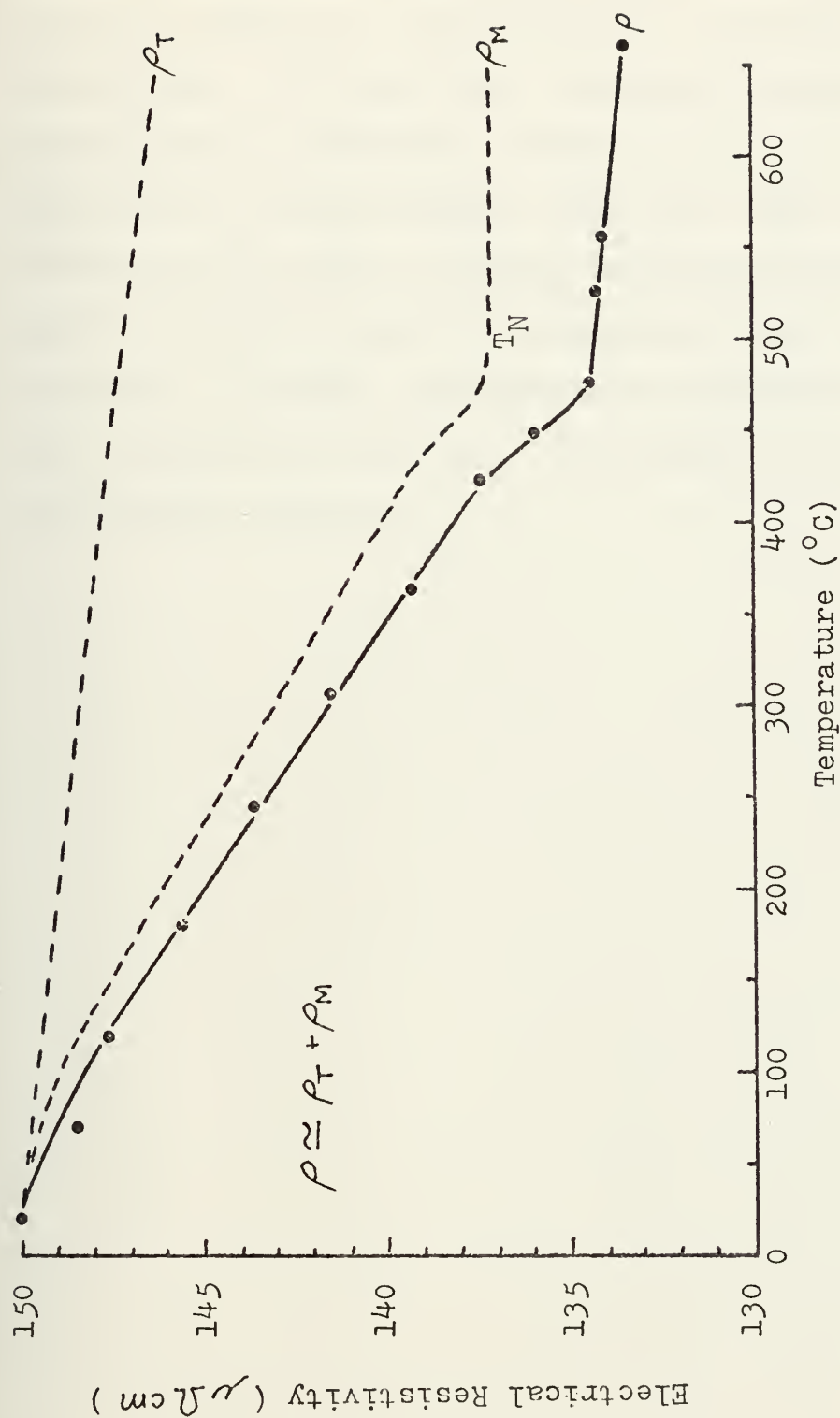


FIGURE 24. Resistivity versus Temperature for Incramute (alloy previously Solutionized at 700° C (for 40 Min)).

The rate at which the compositional changes occur depends on the rate that the sample is being heated. More rapid heating, therefore, would result in a different Néel temperature. This test was conducted at an approximate heating rate of 50°C/min. Ideally, for an alloy consisting of a single metallic compound, there would be no compositional change occurring during heating and the antiferromagnetic disorder temperature would be clearly definable. The Néel temperature determined for Incramute must be considered as only a starting point for further experimental efforts.

V. CONCLUSIONS

1. The heat treatment of Incramute, required to achieve optimum damping capacity, is very sensitive to the aging temperature for fixed aging time.
2. Applied tensile stress during aging retards the aging kinetics of Incramute, lowering it's damping capacity, by reducing the amount of martensite that forms during quenching.
3. Applied tensile stress during quenching retards the formation of martensite as exhibited by the reduction in the martensitic transformation temperature.
4. The martensite transformation temperature is a linear function of the stress applied during cooling (increasing the applied tensile stress proportionately reduced T_{P-M}).
5. The SDC of Incramute can be consistently explained by assuming that damping is a function of the volume of martensite formed as a result of heat treatment given. Low shear stress damping tests indicate that the highest SDC values occur for the most highly martensitic specimens. High shear stress damping tests indicate that the highest SDC value occur for an optimum volume of martensite.
6. The use of electrical resistivity is an excellent parameter to use in measuring the aging kinetics of Incramute. Its usefulness, however, in analyzing the quenching process is limited primarily because of

relatively small difference between the resistivities of the parent and martensitic phases.

VI. RECOMMENDATIONS

1. Microscopic and diffraction studies should be made to:

a. Identify the diffusive processes that occur during the aging process.

b. Precisely identify the relationship between SDC and the potential energy absorption phenomena (intramartensite twin boundary motion, intermartensite boundary motion, and interphase boundary motion).

c. Validate the M_s data accumulated during this research.

2. Further studies should be made to clarify the relationship between the amount of martensite contained in Inframute at room temperature and its specific damping capacity as determined by a range of applied torsional stresses.

APPENDIX

A. UNCERTAINTY ANALYSIS [12] :

1st W_i = uncertainty of component

then

$$W_A = A \left[\sum_{i=1}^n a \frac{W_i}{X_i} \right]^{1/2}$$

where A = component value

X_i = value of subcomponent i whose uncertainty is

a = exponent of subcomponent

1. Resistivity (as plotted):

1st R = measured resistance

L = measured length

D = measured diameter

T = temperature (readability)

r = resistance (readability)

T_c = temperature (thermocouple)

ρ = computed resistivity

$$\text{Then } \frac{W_\rho}{\rho} = \left[\left(\frac{W_R}{R} \right)^2 + \left(\frac{W_L}{L} \right)^2 + \left(\frac{2W_D}{D} \right)^2 + \left(\frac{W_T}{T} \right)^2 + \left(\frac{W_r}{R} \right)^2 + \left(\frac{W_{TC}}{T} \right)^2 \right]^{1/2}$$

$$\text{Example: } \frac{W_\rho}{130 \times 10^{-6}} = \left[\left(\frac{1.0 \times 10^{-6}}{0.0051} \right)^2 + \left(\frac{1.0 \times 10^{-3}}{2.747} \right)^2 + \left(\frac{2(2 \times 10^{-4})}{0.2018} \right)^2 + \left(\frac{3}{500} \right)^2 + \left(\frac{0.8}{130} \right)^2 + \left(\frac{2}{150} \right)^2 \right]^{1/2}$$

$$W_\rho = 130 \times 10^{-6} [9.69 \times 10^{-3}] = 1.26 \mu \Omega \text{ cm}$$

B. SPECIFIC DAMPING CAPACITY (as plotted)

$$SDC = \frac{A_1^2 - A_n^2}{NA_1^2} \times 100 \quad \text{and} \quad S = \frac{T_c}{J}$$

Let A_1 = amplitude of first cycle
 A_n = amplitude of nth cycle
 N = number of cycles covered (n-1)
 T = torque
 c = $D/2$
 S = surface shear stress
 $J = \frac{\pi D^4}{32}$

then $W_{SDC} = SDC \left[\left(\frac{2W_{A1}}{A_1} \right)^2 + \left(\frac{-2W_{An}}{A_n} \right)^2 + \left(\frac{W_S}{S} \right)^2 \right]^{1/2}$

where $W_S = S \left[\left(\frac{2W_c}{D} \right)^2 + \left(\frac{-2W_{An}}{A_n} \right)^2 + \left(\frac{W_T}{T} \right)^2 \right]^{1/2}$

example: $W_S = 5 \times 10^{-3} \left[\left(\frac{2(1 \times 10^{-4})}{0.2018} \right)^2 + \left(\frac{4(2 \times 10^{-4})}{0.2018} \right)^2 + \left(\frac{-0.005}{1.958} \right)^2 \right]^{1/2}$

$$W_S = 5 \times 10^{-3} [4.28 \times 10^{-3}]^{1/2} = 24 \text{ psi}$$

$$W_{SDC} = 25.6 \left[\left(\frac{2(0.02)}{5.08} \right)^2 + \left(\frac{-2(0.02)}{4.38} \right)^2 + \left(\frac{24.0}{5000} \right)^2 \right]^{1/2}$$

$$W_{SDC} = 25.6 [0.013] = 0.333 \%$$

C. TABULATED UNCERTAINTIES

Resistivity Data:

| <u>Term</u> | <u>Uncertainty</u> | <u>Units</u> |
|----------------|--------------------|--------------|
| R | 1.0 | |
| W _L | 0.001 | in. |
| D | 0.0002 | in. |
| T | 3 | °C |
| r | 0.8 | |
| TC | 2 | °C |

SDC Data:

| | | |
|----------------|--------|-----------|
| A ₁ | 0.2 | divisions |
| A ₂ | 0.2 | divisions |
| N | 0 | cycles |
| T(100 psi) | 0.0001 | lbf•in |
| T(500 psi) | 0.005 | lbf•in |
| T(10,000 psi) | 0.005 | lbf•in |
| S(1000 psi) | 4.12 | psi |
| S(5000 psi) | 24.0 | psi |
| S(10,000 psi) | 42.8 | psi |

LIST OF REFERENCES

1. Hills, N.A., A Study of the Influence of Stress and Temperature on Damping Capacity of Mn-Cu Alloys for Ship Silencing Applications, M.S. Thesis, Naval Postgraduate School, Monterey, California, 1974.
2. Naval Postgraduate School Report NPS-59Ps 74061, Materials Approaches to Ship Silencing, by Perkins, J., Edwards, G.R., Hills, N.A., June 1974.
3. United States Department of the Interior Bureau of Mines Bulletin 624, Manganese-Copper Damping Alloys, by Jensen, J.W., Walsh, D.F., 1965.
4. Michels, W.C., Advanced Electrical Measurements, p. 18-22, D. Van Nostrand, 1965.
5. Faires, V.M., Design of Machine Elements, p. 211-216, Macmillan, 1965.
6. Stone Manganese Marine Limited Technical Brief No. 7, Sonostom High Damping Capacity Alloy, p. 6.
7. Naval Ship Research and Development Center Unclassified Letter NP/10310(2814 E) Report 8-975 to Naval Ship Systems Command, Subject: Corrosion Behavior of Manganese-Copper-Vanadium alloy, 16 Nov. 1971.
8. Trona Chemicals, American Potash & Chemical Corporation Letter to Naval Ship Research & Development Lab., subject: Conclusions from Research Program at Battelle with various Mn-Cu alloys, 28 April 1970.
9. Patel, J.R., Cohen, M., "Criterion for the Action of Applied Stresses in the Martensitic Transformation," ACTA Metallurgica, v. 1, p. 331, Sept. 1953.
10. Chalmer, B. and Quarrel, A.G., The Physical Examination of Metals, 2d ed., Edward Arnold Ltd., 1960.
11. Weiss, R.J., Solid State Physics For Metallurgists, v. 6, Addison-Wesley, 1963.
12. Holman, J.P., Experimental Methods for Engineers, p. 37-40, McGraw-Hill, 1966.
13. Warlimont, H., Delaey, L., Krishnan, R.V., Tas, H., "Thermoelasticity, Pseudoclasticity and the Memory Effects Associated with Martensitic Transformations, Part 3: Thermodynamics and Kinetics, Journal of Materials Science, v. 9, p. 1545-1555, 1974.

14. Perkins, J., Edwards, G.R., Johnson, J.M., and Allen, R.R., "Thermomechanical Characteristics of Alloys Exhibiting Martensitic Thermolasticity," paper presented at Symposium on Shape Memory Effects and Applications, 7th Annual TMS-AIME Spring Meeting, University of Toronto, Canada, May 18-22, 1975.
15. Cohen, M., Machlin, E.S., Paranjpe, V.G., "Thermodynamics of the Martensitic Transformation," Thermodynamics in Physical Metallurgy, ASM, p. 242-243, 1950.
16. Averbach, B.L., "The Effect of Plastic Deformation on Solid Reactions," Cold Working of Metals, p. 264.
17. Warlimont, H., Delaey, L., Erishnan, R.V., Tas, H., "Thermoplasticity, Pseudoelasticity and the Memory Effects Associated with Martensitic Transformations, Part 2: The Macroscopic Mechanical Behavior," Journal of Materials Science, v. 9, p. 1542, 1974.
18. Sugimoto, K., Mori, T., Shiode, S., "Effect of Composition on the Internal Friction and Young's Modulus in - Phase Mn-Cu Alloys," Metal Science Journal, p. 103, v. 7, 1973.

INITIAL DISTRIBUTION LIST

| | No. Copies |
|---|------------|
| 1. Defense Documentation Center Cameron Station Alexandria, Virginia 22314 | 2 |
| 2. Library, Code 0212 Naval Postgraduate School Monterey, California 93940 | 2 |
| 3. Chairman, Code 59 Department of Mechanical Engineering Naval Postgraduate School Monterey, California 93940 | 2 |
| 4. Capt. L. H. Beck, Code 037 Naval Ship Systems Command Ship Silencing Program Washington, D.C. 20350 | 1 |
| 5. Mr. S. M. Blazek Naval Ship Systems Command Ship Silencing Program Washington, D.C. 20350 | |
| 6. Mr. E. J. Czyryca Naval Ship Research and Development Laboratory Annapolis, Maryland 21402 | 1 |
| 7. Professor A. J. Perkins Department of Mechanical Engineering Naval Postgraduate School Monterey, California 93940 | 5 |
| 8. Professor G. R. Edwards Department of Mechanical Engineering Naval Postgraduate School Monterey, California 93940 | 5 |
| 9. Lt. F. L. Youngblood SMC 1640 Naval Postgraduate School Monterey, California 93940 | 5 |

Thesis

161190

Y73 Youngblood

c.1 Characterizing and
controlling the metal-
lurgical properties of a
Cu-Mn alloy for ship
silencing applications.

26 JAN 82

28472

Thesis

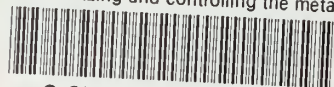
161190

Y73 Youngblood

c.1 Characterizing and
controlling the metal-
lurgical properties of a
Cu-Mn alloy for ship
silencing applications.

thesY73

Characterizing and controlling the metal



3 2768 001 90554 0

DUDLEY KNOX LIBRARY